NASA Contractor Report 4094

Development of a P-I-N HgCdTe Photomixer for Laser Heterodyne Spectrometry

Peter R. Bratt

Hughes Aircraft Company
Santa Barbara Research Center
Goleta, California

Prepared for
Langley Research Center
under Contract NAS1-16057

National Aeronautics
and Space Administration

**Scientific and Technical
Information Office**

1987

CONTENTS

ILLUSTRATIONS

ILLUSTRATIONS (CONT)

TABLES

Section 1
INTRODUCTION

Interest in the development of improved HgCdTe p-i-n photomixer technology was stimulated by NASA's desire to perform environmental remote sensing experiments employing laser heterodyne spectrometry. System requirements included increased bandwidth out to 5 GHz, improved effective heterodyne quantum efficiency to greater than 50%, and reproducible device characteristics for optimum impedance matching to low noise preamplifiers.

The overall objective of this contract was to approach the problem of improving the photomixer performance and reproducibility by designing a new type of photomixer based on the development of a p-i-n HgCdTe device technology.

The work was carried out in two phases. The goals for Phase I were: a bandwidth of 2 GHz, an effective heterodyne quantum efficiency of 30% while operating at 77K and at a wavelength of 10.6 μm, shot noise limited operation for local oscillator power in the range 0.1 to 1.0 mW, and a device diameter no smaller than 100 μm. As evidence of the results achieved, eight photomixers were to be delivered at the end of the Phase I effort.

The goals for Phase II were: a bandwidth of 2.5 GHz, an effective heterodyne quantum efficiency of 50%, and the same operating conditions as above for Phase I. An additional task for Phase II was to build a breadboard model cold GaAs FET preamplifier and evaluate in concert with a HgCdTe photomixer. Deliveries on Phase II again included eight photomixers, one of which was to be installed in a suitable LN_2 dewar along with the cold GaAs FET preamplifier.

Section 2
PHOTOMIXER PERFORMANCE ANALYSIS

To lay down the groundwork for understanding the operation of high frequency photomixers, we start off this section by introducing the fundamental concepts involved in heterodyne detection with a photomixer diode. The theoretical performance limit for noise equivalent power (NEP) is derived and those photomixer parameters which are important for high frequency operation are discussed. Further analysis leads to a theroretical formula for photomixer NEP as a function of frequency which is used to calculate anticipated photomixer performance in the GHz frequency range. This expression will also be useful to evaluate the performance of real photomixers which were fabricated for this program.

2.1 HETERODYNE DETECTION

Heterodyne detection requires the superposition of two optical beams on the detector such as shown in Figure 2-1. One is the signal beam and the other is called the local oscillator beam. Consider two plane polarized beams with E field vectors parallel to the plane of the detector and to each other. Let E_s represent the signal field with angular frequency ω_s and E_{LO} the local oscillator field with frequency ω_{LO}. The total field is then

$$E(t) = E_s \cos \omega_s t + E_{LO} \cos \omega_{LO} t. \qquad (1)$$

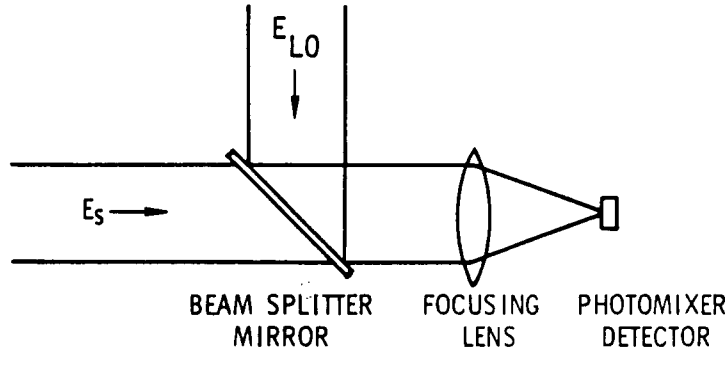

Figure 2-1. Illustration of a Method for Superposition of Two Optical Beams on a Detector

By Poynting's theorem, the total power incident on the detector area A is given by

$$P(t) = \frac{E^2(t)\, A}{z_o}, \tag{2}$$

where z_o is the impedance of free space.

This power will produce a current in the detector, which is presumed to be a photodiode and is also called the photomixer,

$$i(t) = \frac{e\, \eta\, P(t)}{h\nu} \tag{3}$$

where η is the quantum efficiency which has been assumed to be constant over the detector area, and the other symbols have their usual meanings.

Combining equations (1) and (2) into (3) yields

$$\begin{aligned} i(t) &= \frac{e\, \eta\, A}{z_o h\nu} \left[E_s \cos \omega_s t + E_{LO} \cos \omega_{LO} t\right]^2 \\ &= \frac{e\, \eta\, A}{z_o h\nu} \left[\frac{1}{2} E_s^{\,2} (1 + \cos 2\, \omega_s t) + \frac{1}{2} E_{LO}^{\,2} (1 + \cos 2\, \omega_{LO} t)\right. \\ &\quad \left. + E_s\, E_{LO} \cos (\omega_s - \omega_{LO}) t + E_s\, E_{LO} \cos (\omega_s + \omega_{LO}) t\right]. \end{aligned} \tag{4}$$

The cosine terms in ω_s and $\omega_s + \omega_{LO}$ correspond to oscillations at optical frequencies which the detector cannot follow. Therefore, the detector only responds to the dc parts of these terms and they create dc currents given by

$$I_s = \frac{e\, \eta\, A}{2 z_o h\nu} E_s^{\,2} \tag{5}$$

and

$$I_{LO} = \frac{e\, \eta\, A}{2 z_o h\nu} E_{LO}^{\,2}. \tag{6}$$

In the usual case, I_{LO} is much greater than I_s because E_{LO} is much greater than E_s.

The difference frequency $(\omega_s - \omega_{LO})$ may be orders of magnitude less than either ω_s or ω_{LO} so it can be followed by the detector. This difference frequency is usually called the intermediate frequency $\omega_{IF} = \omega_s - \omega_{LO}$.

Equation (4) can now be represented by

$$i(t) = I_s + I_{LO} + 2\sqrt{I_s I_{LO}} \cos \omega_{IF} t. \tag{7}$$

The information which was incorporated in the signal beam has been transferred to the intermediate frequency. Therefore, the IF current is the quantity of interest for calculating signal-to-noise ratios.

The signal-to-noise power at the output of the detector will be given by

$$\left(\frac{S}{N}\right)_p = \frac{\overline{i_{IF}^2}}{\overline{i_n^2}}, \tag{8}$$

where

$$\overline{i_{IF}^2} = \overline{\left(2\sqrt{I_s I_{LO}}\right)^2 \cos^2 \omega_{IF} t} = 2 I_s I_{LO}. \tag{9}$$

If the detector is shot noise limited, then

$$\overline{i_n^2} = 2eIB, \tag{10}$$

where I is the total current passing through the detector and B is the electrical bandwidth of the IF amplifier. To maximize signal to noise, it is desired to have I_{LO} dominate the detector current. Therefore, the noise becomes

$$\overline{i_n^2} = 2eI_{LO}B, \tag{11}$$

and the signal-to-noise ratio is

$$\left(\frac{S}{N}\right)_p = \frac{2I_s I_{LO}}{2eI_{LO}B} = \frac{I_s}{eB}. \tag{12}$$

Since $I_s = e\,\eta\,P_s/h\nu$, this becomes

$$\left(\frac{S}{N}\right)_p = \frac{\eta P_s}{h\nu B}. \tag{13}$$

The noise equivalent power (NEP) is then

$$NEP = \frac{P_s}{(S/N)_p} = \frac{h\nu B}{\eta}. \tag{14}$$

An ideal heterodyne detector ($\eta = 1$) operating at 10.6 μm should therefore have an NEP of

$$NEP = 1.9 \times 10^{-20} \text{ B}.$$

A real detector will always fall short of this ideal limit by some degree. In the real situation, a number of other factors must be considered such as LO and signal mixing efficiency, dark current noise, effect of amplifier noise, and detector quantum efficiencies less than unity. These factors are introduced into the analysis in the following subsections.

2.2 HETERODYNE MIXING EFFICIENCY

The previous treatment of heterodyne photomixing assumed perfect phase matching of the signal and LO wave fronts at the detector. In general, the wave fronts are not perfectly matched over the entire sensitive area. Usually, the signal field at the detector is an Airy diffraction pattern and the LO field may or may not be an Airy pattern. A tilt angle between signal and LO beams will also contribute to phase mismatch. In addition, variations in detector quantum efficiency over the detector surface will affect mixing efficiency.

These considerations have been treated in detail in the literature.[1,2] It turns out that these effects can be incorporated into the signal-to-noise expression, equation (13), as simple multiplicative factors. Thus,

$$\left(\frac{S}{N}\right)_p = \frac{P_s m \eta_{eff}}{h\nu B}, \tag{15}$$

where m represents the mixing efficiency due to mismatch between signal and LO wave fronts, and η_{eff} takes into consideration variations in detector quantum efficiency across the surface. For well-designed systems, m is in the range 0.7 to 0.8 and η_{eff} depends on detector construction. Typical values for η_{eff} may range from 0.4 to 0.8.

2.3 PHOTOMIXER FREQUENCY RESPONSE

The primary limitations to the high-frequency response of a photomixer are as follows:

1. Diffusion of carriers to p-n junction

2. Drift of carriers across the junction depletion region

3. Junction capacitance

Each of these mechanisms will now be discussed and an analysis made to determine their relative importance.

2.3.1 Diffusion Limits

Photogenerated minority carriers which are produced some distance away from the p-n junction must diffuse to the junction before they can be "counted" as photocurrent. This diffusion process requires a certain amount of time. The situation is illustrated in Figure 2-2 for the case of present n^+-n-p photomixers.

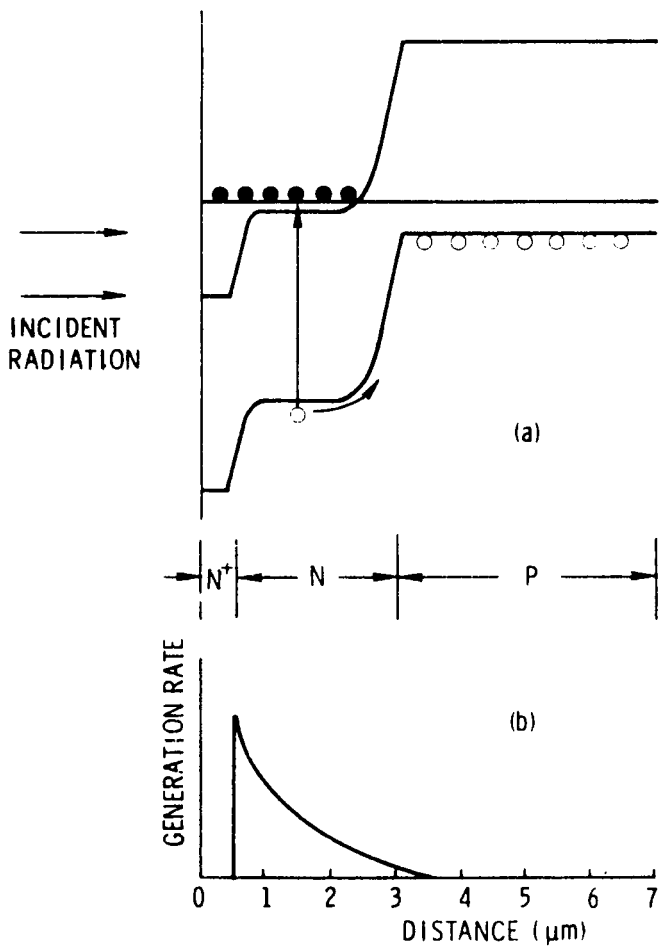

Figure 2-2. Illustration of Minority Carrier (Hole) Generation in N-Region and Diffusion to P-N Junction. (a) Energy Band Diagram; (b) Relative Hole Generation Rate versus Distance into Crystal

The frequency response for the diffusion limited photodiode has been treated by Sawyer and Rediker.[3] They found that the upper limit to the frequency response (0.707 point) is given approximately by

$$f_c = \frac{2.4D}{2\pi d^2}, \tag{16}$$

where d is the distance from the point of origin of the minority carriers to the junction; and D is the diffusion coefficient, given by

$$D = \mu \frac{kT}{e}. \tag{17}$$

On the n-side of the junction, the minority carriers are holes which have a mobility of about 800 cm^2/V-sec at 77K which gives D_p = 5.3 cm^2/sec. Assuming that the distance $d = 1/\alpha \approx 2 \times 10^{-4}$ cm, we find that f_c = 51 MHz. It is clear that slow diffusing holes can cause a frequency response component far below the desired 2 GHz region.

On the p-side of the junction, the minority carriers are electrons with a mobility of about 1.5×10^5 cm^2/V-sec at 77K which gives $D_n = 10^3$ cm^2/sec. Assuming again that these electrons must diffuse a distance $d = 1/\alpha \approx 2 \times 10^{-4}$ cm to reach the junction, we have f_c = 9.6 GHz. Thus, the faster diffusing electrons should not degrade the frequency response of the photomixer diode.

2.3.2 Drift Limit

This situation occurs when photogenerated carriers are produced within the depletion region of a p-n junction and are then swept out by the large electric field existing there. This type of junction is illustrated in Figure 2-3. Such a structure may be realized in p-i-n or graded junction devices. This case has been analyzed by Gartner,[4] who shows that the upper frequency limit (0.707 point) is

$$f_c = \frac{2.8v}{2\pi W}, \tag{18}$$

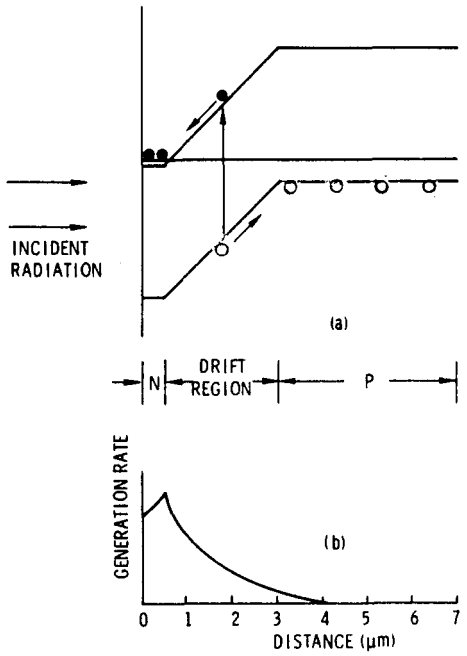

Figure 2-3. Illustration of Carrier Generation in a Drift Limited Diode. (a) Energy Band Diagram; (b) Relative Generation Rate versus Distance into the Crystal

where v is the carrier velocity and W the width of the depletion region. Assuming $W = 1/\alpha \approx 2 \times 10^{-4}$ cm and $v = 5 \times 10^{6}$ cm/sec, we find that $f_c = 11$ GHz. Thus, drift limitations should not degrade the frequency response.

2.3.3 Capacitance Limit

The equivalent circuit for a photomixer diode is shown in Figure 2-4. The series inductance L is negligible in the diode itself but the output leads from the diode may contribute appreciable amounts of inductance. In the GHz frequency region, lead inductance may be important, so L should not be neglected. Analysis of the circuit of Figure 2-4 shows that the IF power delivered to the load (the preamplifier) is given by*

$$P_{IF} = \overline{i_{IF}^2} R_\ell \frac{|Z_d|^2}{|Z_d + Z_s + Z_\ell|^2}, \tag{19}$$

*See Appendix A for a complete analysis of the photodiode circuit.

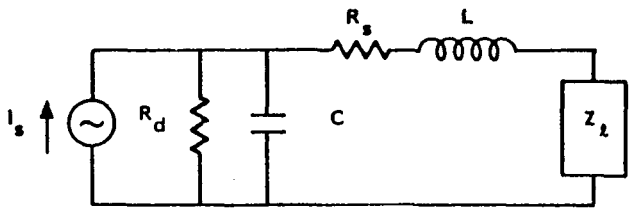

Figure 2-4. Equivalent Circuit for a Photomixer Diode

where

$$Z_d = \frac{R_d}{1 + j\omega C R_d}$$

$$Z_s = R_s + j\omega L$$

$$Z_\ell = R_\ell$$

and we have assumed the load impedance is a real number. Rationalizing the complex terms and taking absolute values gives the expression

$$P_{IF} = \overline{i_{IF}^2} R_\ell F(\omega), \tag{20}$$

where the term $F(\omega)$ contains the frequency dependence due to circuit capacitance and inductance,

$$F(\omega) = \left\{\left[\left(\frac{R_s + R_\ell}{R_d}\right) + 1 - \omega^2 LC\right]^2 + \left[\frac{\omega L}{R_d} + \omega C(R_s + R_\ell)\right]^2\right\}^{-1}. \tag{21}$$

For the case $L = 0$, this reduces to

$$F(\omega) = \left\{\left[\left(\frac{R_s + R_\ell}{R_d}\right) + 1\right]^2 + \left[\omega C(R_s + R_\ell)\right]^2\right\}^{-1}. \tag{22}$$

Usually $R_d >> (R_s + R_\ell)$ so equation (22) can be approximated by

$$F(\omega) \approx \left\{1 + \left[\omega C(R_s + R_\ell)\right]^2\right\}^{-1} \tag{23}$$

From this, we can see that the 3 dB frequency where the IF signal power to the load is decreased by a factor of two is

$$f_c = \frac{1}{2\pi C(R_s + R_\ell)}. \tag{24}$$

As an example, consider a case where $R_s = 10\Omega$, $R_\ell = 50\Omega$ and we want f_c to be 2 GHz or greater. Equation (24) then gives the result that C must be less than 1.3 pF.

The foregoing analysis has shown that, to obtain a photomixer with speed of response extending to 2 GHz, a drift type photodiode structure must be employed and the p-n junction capacitance (plus any stray shunt capacitance) must be kept small. The required small capacitance can only be obtained by using HgCdTe with a very low impurity doping concentration in the junction so as to provide a wide depletion layer. The p-n junction capacitance is given by

$$C_j = \kappa\varepsilon_o \frac{A}{W}, \tag{25}$$

where κ is the dielectric constant of HgCdTe ($\kappa = 18$), ε_o is the permittivity of empty space, A is the junction area, and W the depletion layer width.

For the usual case of a one-sided step junction, W is given by[5]

$$W = \left[\frac{2\kappa\varepsilon_o}{eN}\left(\phi_b + V_R\right)\right]^{1/2}, \tag{26}$$

where N is the impurity doping on the lightly doped side (n-type side in our case), ϕ_b is the junction built-in voltage, and V_R is the reverse bias voltage. Thus depletion layer width and, hence, capacitance are controlled by donor doping and reverse bias voltage.

Figure 2-5 shows how both depletion layer width and capacitance depend on these parameters. Assuming a capacitance of 1 pF is required and the junction area is 2×10^{-4} cm^2, then the capacitance per unit area is 5×10^{-9} F/cm^2. Figure 2-5 shows that, if reverse bias voltage is to be kept below 1V, the

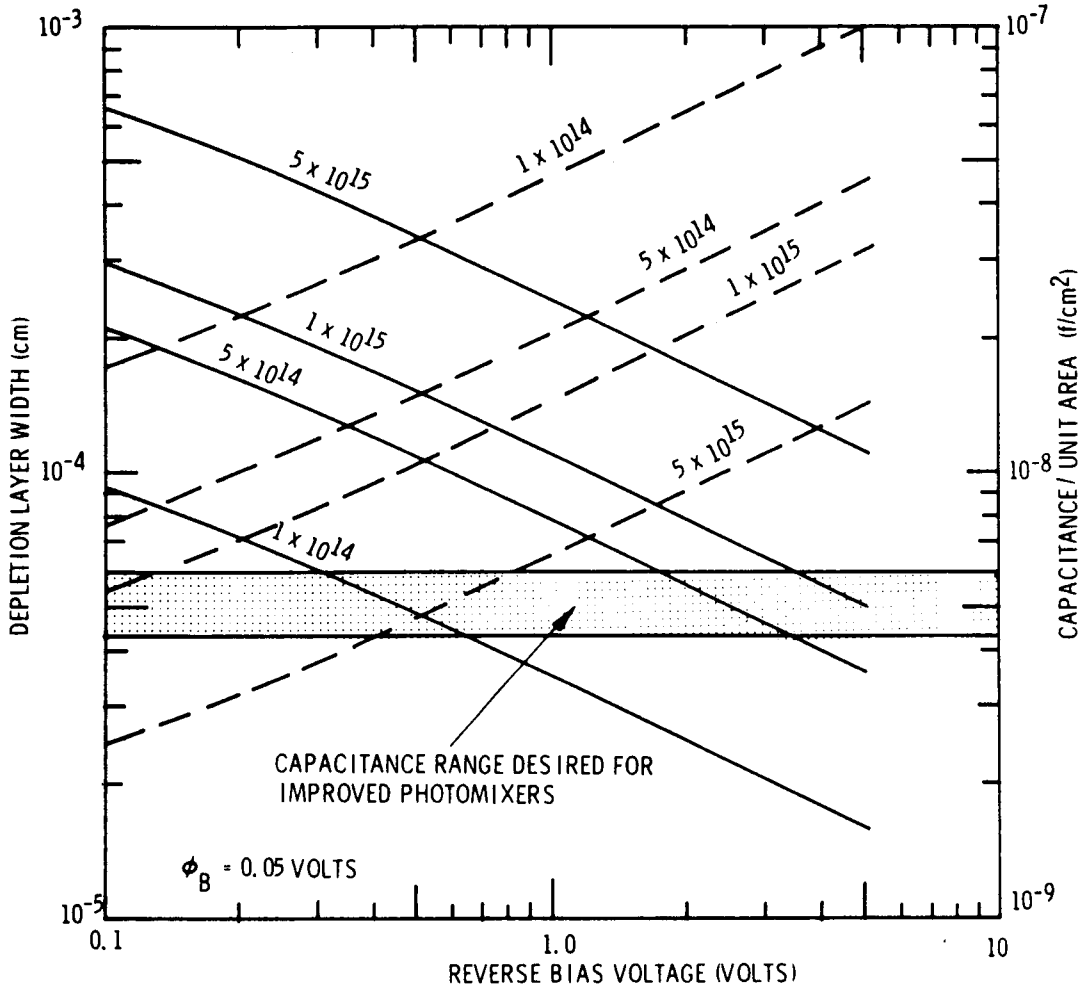

Figure 2-5. Calculated Variation of Depletion Layer Width and Capacitance versus Reverse Bias Voltage with Donor Doping Concentration as a Parameter. Dashed curves represent depletion layer width. Solid curves represent capacitance per unit area.

donor doping must be less than about $2 \times 10^{14}/cm^3$. The depletion layer width, in this case, will be on the order of 3 to 4 μm. Reverse bias voltages greater than about 1V are difficult to achieve in narrow bandgap HgCdTe alloys because of avalanche breakdown and excessive leakage conductance. Therefore, a design that is based on low doping concentrations is the only viable approach to increased frequency response.

2.4 HETERODYNE NEP

The heterodyne NEP for an ideal detector whose only source of noise is the shot noise induced by the local oscillator was derived previously as equation (14). For a real detector we must also consider other sources of noise. The other two main contributions to the noise come from the dark current shot noise and the preamplifier noise. Including these two additional noise terms along with the LO produced shot noise, an expression for the real detector heterodyne NEP may be derived which is*

$$NEP_H = \frac{h\nu B}{\eta_{eff}^m} \left[1 + \frac{I_d}{I_{LO}} + \frac{N_a(\omega)}{2eR_\ell I_{LO} F(\omega)}\right], \tag{27}$$

where I_d is the photomixer dark current, N_a is the preamplifier noise power, k is Boltzmann's constant, $F(\omega)$ was defined by equation (21), and the other symbols are as previously defined. From this equation, it can be seen that, to minimize NEP_H, one wants to minimize dark current I_d and the preamplifier noise N_a, and increase the local oscillator power so that I_{LO} is large, thereby making the second and third terms in equation (27) much less than unity. In a real detector, there are limits to the amount of LO power which can be applied because of saturation effects. Thus, it is important to minimize I_d and N_a.

An alternate, simplified expression for the heterodyne NEP is sometimes written as

$$NEP_H = \frac{h\nu B}{\eta_H}, \tag{28}$$

where η_H is called the "heterodyne quantum efficiency" and includes all the effects which cause a real detector to fall short of the ideal performance; i.e., optical quantum efficiency, mixing efficiency, and excess noise contributions,

$$\eta_H = \frac{\eta_{eff}^m}{\left[1 + \frac{I_d}{I_{LO}} + \frac{N_a(\omega)}{2eR_\ell I_{LO} F(\omega)}\right]}. \tag{29}$$

*See appendix B for a derivation of the NEP_H equation.

Section 3
PHOTOMIXER DESIGNS

3.1 DIFFUSED JUNCTION DESIGN

Previous work on HgCdTe photomixer diodes at other laboratories employed a planar diffused junction technology. With this design approach, an n^+-n-p^+ structure is produced by in-diffusion of Hg into p-type base material which contains on the order of $10^{17}/cm^3$ Hg vacancies. The in-diffused Hg fills the vacancies and the diffused layer becomes n-type by virtue of residual donor impurities in the crystal. Thus, the resultant donor doping is dependent on purity of the starting material. Extreme care must be exercised in preparation of the HgCdTe base material to obtain the low donor concentrations desired for high-frequency photomixer diodes.

One attempts to adjust the diffusion time and temperature such that the p-n junction is located a distance $1/\alpha$ below the top surface (where α is the absorption coefficient). Thus, the incoming signal radiation is absorbed mainly on the n-type side of the junction. Since $\alpha \approx 5 \times 10^3$ cm^{-1}, the junction depth should be located about 2 μm below the top surface.

A thin n^+ layer is usually produced on top of the n-type region to reduce the sheet resistance between the junction and the top contact. This layer has the added feature of reducing front surface recombination because a barrier is established which inhibits minority carriers (holes) generated in the n-region from diffusing to the surface. Both ion implantation and indium alloying have been used for this n^+ layer. An energy band diagram representative of this design is shown in Figure 3-1.

This design was first utilized by Spears[6,7,8] of MIT Lincoln Laboratories and later adopted by workers at Honeywell Radiation Center.[9,10] It also is the basis for the work on photomixer diodes done in France at S.A.T. and C.N.R.L.[11] The frequency response of photomixers made by this technique has been pushed out into the 1 to 2 GHz range. However, this appears to be achieved only with great difficulty and a low yield of acceptable devices. This translates into high cost to the user.

During the early stages of this program for NASA we at Santa Barbara Research Center also attempted to make HgCdTe photomixers by the diffused

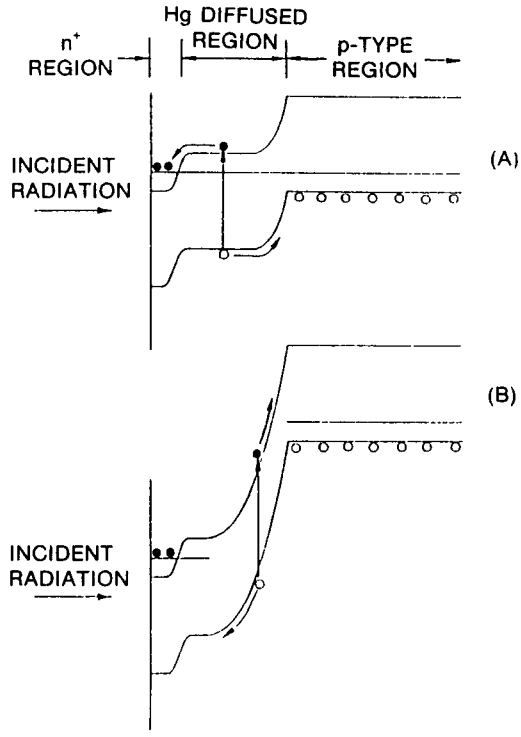

Figure 3-1. Energy Band Diagrams Representing the Hg-Diffused n-p Junction Previously Employed for HgCdTe Photomixers

junction technique. Reasonably good diode characteristics were obtained; however, quantum efficiencies were low due to inability to locate the p-n junction at the proper depth from the top surface. This experience reinforced the previous indications that the diffused junction-technology was difficult to control. Therefore, other process technologies were sought.

3.2 HETEROJUNCTION DESIGN

Another photomixer design approach considered for this program was based on a heterojunction structure formed using a liquid phase epitaxial growth process. The proposed structure is illustrated by the energy band diagram shown in Figure 3.2.

To make this structure, one begins with a p^+ HgCdTe substrate wafer with a wide bandgap. For example, a $Hg_{0.7}Cd_{0.3}Te$ alloy could be used which has a bandgap of about 0.3 eV at 77K. A 4 to 5 μm thick epitaxial layer of lightly n-type or near intrinsic HgCdTe would then be formed on the substrate crystal by liquid phase epitaxial growth. The composition of this epitaxial layer

would be nominally $Hg_{0.8}Cd_{0.2}Te$, and its bandgap would therefore be about 0.1 eV. This would be the photon absorbing region, and it would be sensitive to wavelengths out to about 12 μm. On top of this first epitaxial layer, a second layer is grown. This second layer would be heavily n-type (10^{16} to 10^{17} donor atom/cm^3) and would have a bandgap of about 0.3 eV. This layer will not absorb radiation in the 5 to 12 μm range, and simply acts as a window layer with low sheet resistance. This layer need be only 1 to 2 μm in thickness.

An alternate approach would be to use ion implantation to form the n^+ layer. However, there may be some advantage to the second epitaxial layer in terms of lower surface recombination velocity and better passivation of the diode structure. The main advantage expected to be gained from this technical approach to improved photomixer fabrication is larger reverse breakdown voltages. The p^+-n heterojunction should be less susceptible to avalanche breakdown, particularly if the electrical junction would be located within the metallurgical transition region between the $Hg_{0.7}Cd_{0.3}Te$ and $Hg_{0.8}Cd_{0.2}Te$ alloy layers. The diagram in Figure 3-2 is drawn for this case. A slight

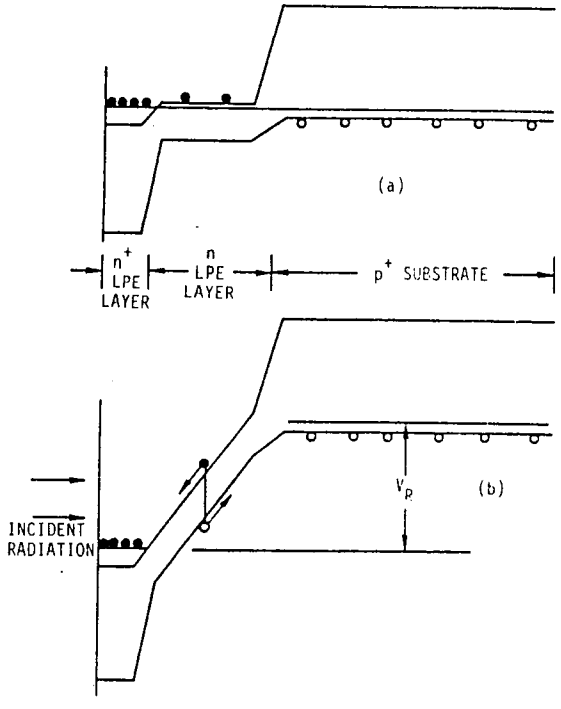

Figure 3-2. Energy Band Diagrams showing Heterojunction Design for an n^+-n-p Photomixer Diode (a) Zero Reverse Bias (b) With Reverse Bias

gradation in the metallurgical transition region should reduce electric field strengths in the p^+-n junction. This could also help to inhibit surface leakage current across the depletion region and decrease surface-originated avalanche breakdown effects.

Another advantage to this proposed structure is that absorption of 10 to 12 μm radiation occurs only in the $Hg_{0.8}Cd_{0.2}Te$ epilayer which is the drift region. Therefore, there can be no slow diffusion effects from carriers generated outside this region. Also, as mentioned previously, the 4 to 5 μm thick epilayer will absorb more of the incoming photons than a 2 μm thick layer, thus increasing quantum efficiency. For example, if $\alpha = 5 \times 10^3 cm^{-1}$, then the fraction of incoming photons absorbed in the epilayer will be

$$1 - \exp(1 - \alpha W) = 1 - \exp(-2.5) = 0.92 \qquad (30)$$

as compared with 0.63 for a 2 μm thick layer.

Although in principle, the heterojunction design approach was very attractive, in practice it could not be developed within the fiscal constraints of this program. The major problems to be solved, i.e., growth of the narrow gap n-HgCdTe on the wide gap p-HgCdTe plus the achievement of very low donor doping ($N_D \approx 1 \times 10^{14} cm^{-3}$) in the narrow gap material, would require an extensive liquid phase epitaxial growth development effort. Therefore, other less expensive design approaches were sought.

3.3 BACKSIDE ILLUMINATED DESIGN

The photomixer design ultimately used for this program was a back side illuminated thin mesa diode structure. This design had been developed during a parallel SBRC IR&D effort. With the inability to obtain deliverable photomixers using the two previously described design approaches, it was decided to employ this alternate design which, besides being quite different from the approaches used in other laboratories, offered a number of advantages over the older diffused junction technology.

The SBRC approach to GHz detector fabrication is illustrated in Figure 3-3. This is called a thin back side illuminated mesa diode configuration. The incident radiation to be detected enters through an Irtran 2 substrate and passes into the HgCdTe through an IR transmitting epoxy. The photodiode is made by ion implanting an n^+ layer on one side of the

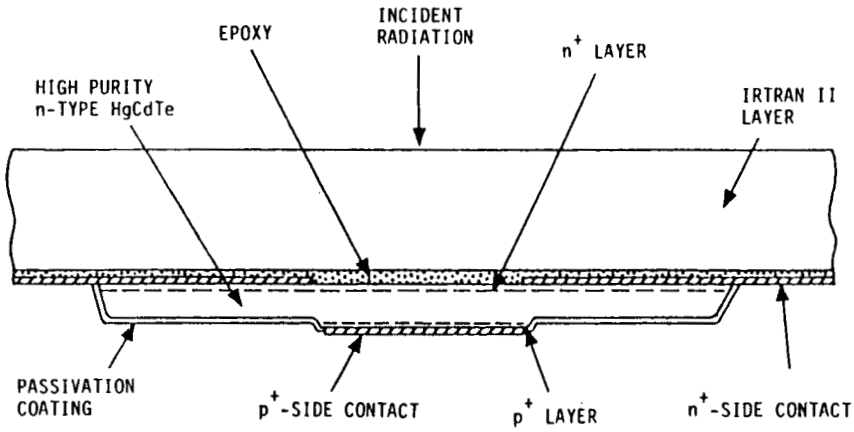

Figure 3-3. GHz PV HgCdTe Detector Cross-Section View

high-purity n-type HgCdTe and forming a p^+ layer on the other. The high-purity HgCdTe active region is approximately 4 μm thick and the n^+ and p^+ regions are each 0.5 μm or less in thickness.

Figure 3-4 shows energy band diagrams which serve to explain the operating principles of the detector. At zero bias, Figure 3-4(a), the device operates in the photovoltaic mode. Minority carriers (holes) generated by photon absorption in the n region must reach the p^+-n junction by diffusion. This, being a relatively slow process, limits the frequency response to about 50 MHz. In reverse bias, Figure 3-4(b), the depletion region at the p^+-n junction widens out and if conditions are right can be made to extend throughout the entire thickness of the n layer. For this case, the free carriers generated within the active region by photon absorption are quickly swept out by the high electric field in the depletion region. Thus the device behaves as a "drift-type" photodiode. The frequency limit for this mode of operation depends on the strength of the electric field which can be achieved in the HgCdTe and is currently about 10 GHz. Thus, other factors, such as junction capacitance and stray inductance and capacitance, control the high-frequency rolloff.

This device configuration incorporates a number of design features which have been intentionally included to optimize high-frequency performance. These features are as follows:

1. The base region thickness can be controlled during processing to provide the optimum tradeoff between optical absorption thickness and depletion layer width.

2. The sensitive area is well defined and unobscured by contact metallization.

3. Low junction capacitance is assured by preselection of low-doped n-type HgCdTe material. This material is readily available from SBRC's high purity crystal inventory produced for phototconductive detector array fabrication.

4. No extra junction area is required for contact metallization which would create additional parasitic capacitance.

5. Reflection of signal radiation off the p-side contact gives a double pass through the HgCdTe enhancing absorption and, thereby, increasing quantum efficiency.

6. The device should have low series resistance because of the low sheet resistance on the n side obtained by the n^+ ion implantation and low resistance on the p side due to its thinness.

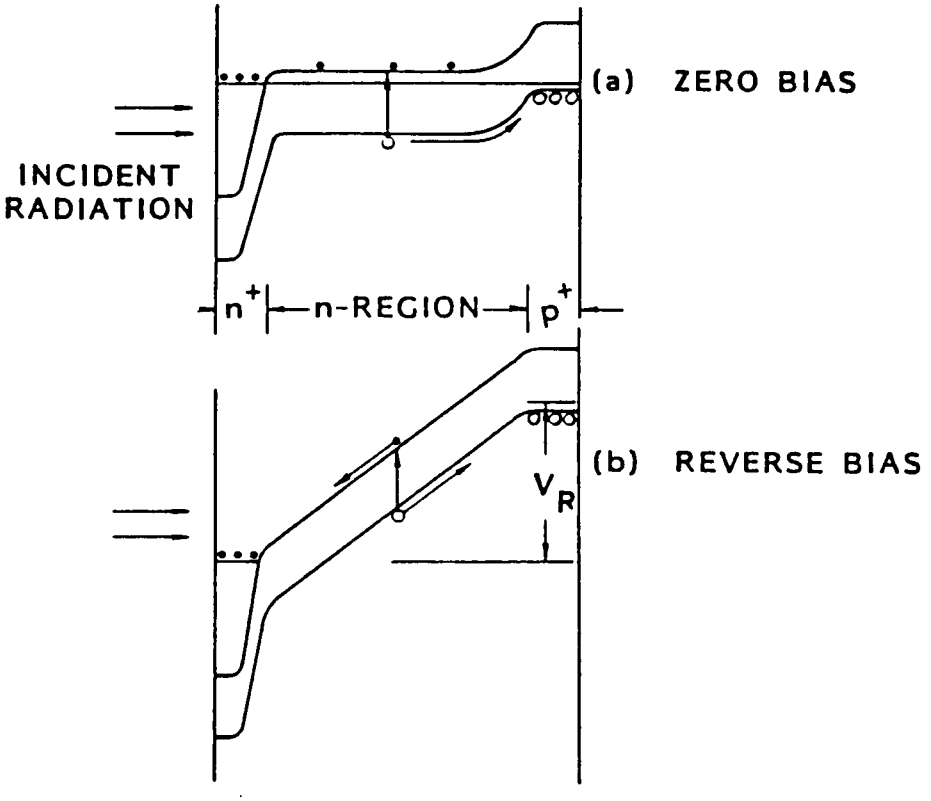

Figure 3-4. Energy Band Diagrams for High-Speed HgCdTe Photodiode with Back Side-Illuminated n^+-n-p^+ Structure

Additional design features which do not bear on high-frequency performance, but are worth noting, are:

1. Because radiation is not directly incident on the p-n junction, the device is potentially more resistant to damage by excessive laser power.

2. The region where the p-n junction comes to the surface is shielded from exposure to visible or ultraviolet radiation which may cause changes in surface leakage currents.

3. The single-element design of Figure 3-2 is easily extended to a close-spaced 2-dimensional array format.

One of the key process technologies required to fabricate this structure is the formation of the p^+-n junction. This junction must be formed after the HgCdTe is epoxy bonded to the Irtran 2 substrate and thinned down. Therefore, no high temperature processes are permitted. On the IR&D program, SBRC developed two methods for the p^+-n junction formation. One employed a low temperature diffusion of Au into the HgCdTe forming a p+ layer and the other employed a Pt metal Schottky barrier. Reasonably good photomixer diodes were fabricated using both techniques.

Section 4
PHOTOMIXER FABRICATION AND TEST

4.1 PHOTOMIXER FABRICATION

The photomixer diodes were fabricated according to the thin backside illuminated mesa structure design described in the previous section. The starting material was high purity n-type HgCdTe grown by SBRC's zone melting technique and selected to have $N_D < 2 \times 10^{14}$ cm^{-3} and a long wave cut-off at 77K of 11.5 to 12 μm. Many diodes were fabricated simultaneously from a single HgCdTe wafer bonded to an Irtran 2 substrate. The fabrication process employed standard HgCdTe polish/etching and photolithographic techniques. After fabrication the diodes were individually probe tested for their current-voltage characteristics at liquid nitrogen temperature. This served as a screening test to determine which diodes might be suitable for final testing as photomixers. After screen testing the wafer was diced up into individual diode chips. Figure 4-1 is a photograph of one of these chips showing the top side.

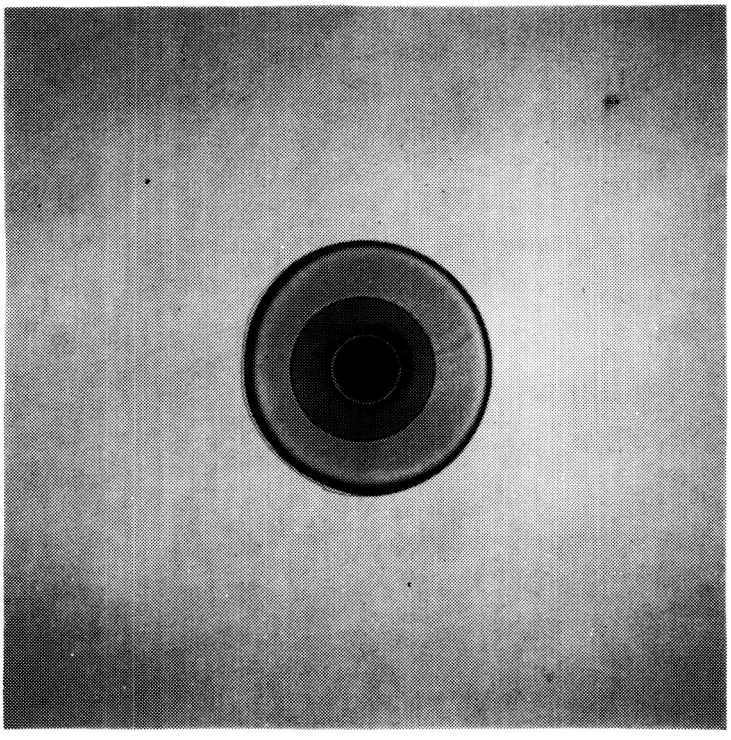

Figure 4-1. Photograph of HgCdTe Photomixer Chip Showing Top Side (Chip Size is 1.5 × 1.5 mm)

These chips were mounted on a Kovar strip which could be attached to a copper heat sink as shown in Figure 4-2. The Kovar strip had a hole machined in it to admit radiation to the back side sensitive region through the Irtran 2 substrate. A short length of 0.001 in. diameter gold wire was connected from the p^+-side of the diode to a small segment of 50Ω ceramic strip line attached to the copper heat sink. Another short length of gold wire was connected from the n^+-side of the diode to the Kovar strip as the ground contact.

For photomixer testing the assembly shown in Figure 4-2 was mounted in an LN_2 test dewar as shown in Figure 4-3. This is an SBRC model 40742 dewar modified for high frequency operation by installation of an SMA 50Ω coaxial feedthrough and a stainless steel 50Ω coaxial line leading directly to the photomixer.

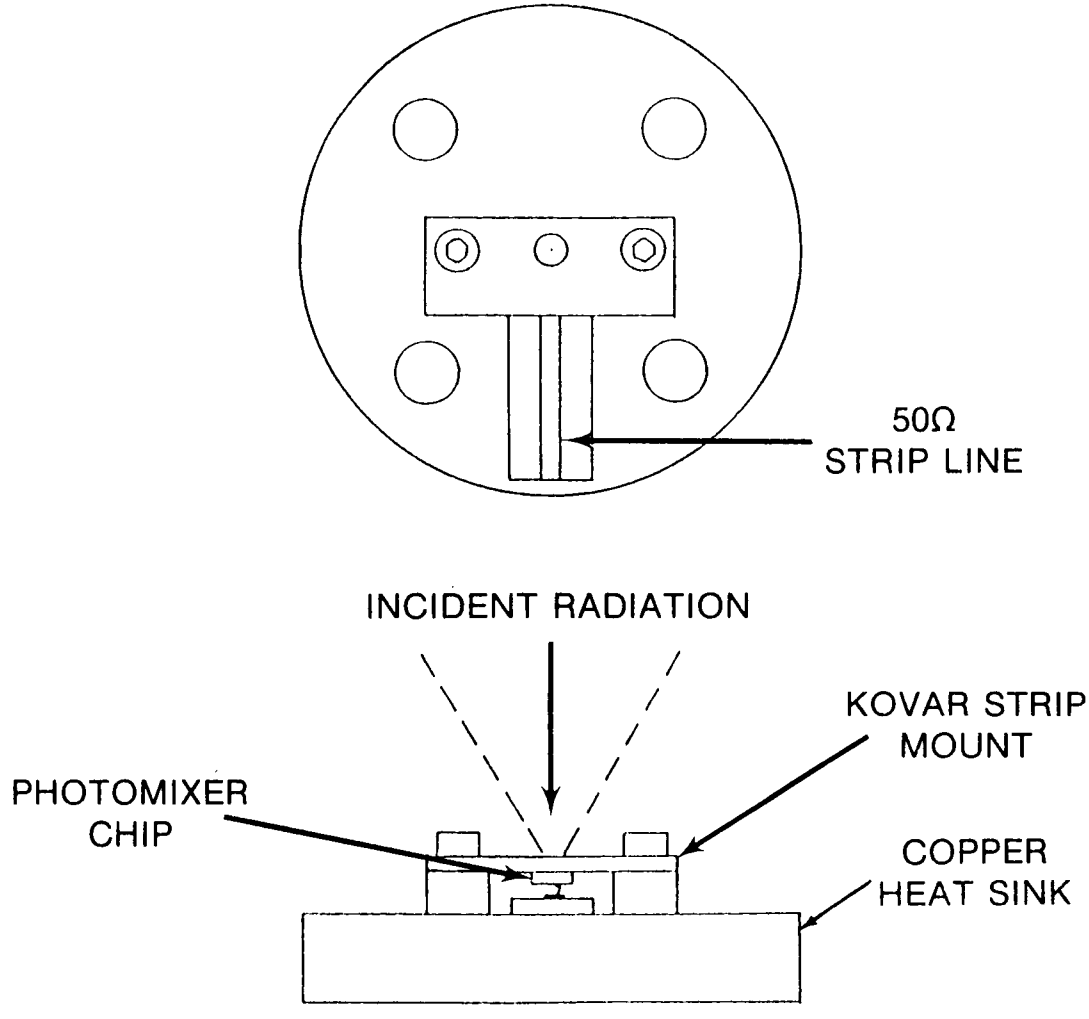

Figure 4-2. Mounting Assembly for HgCdTe Photomixers

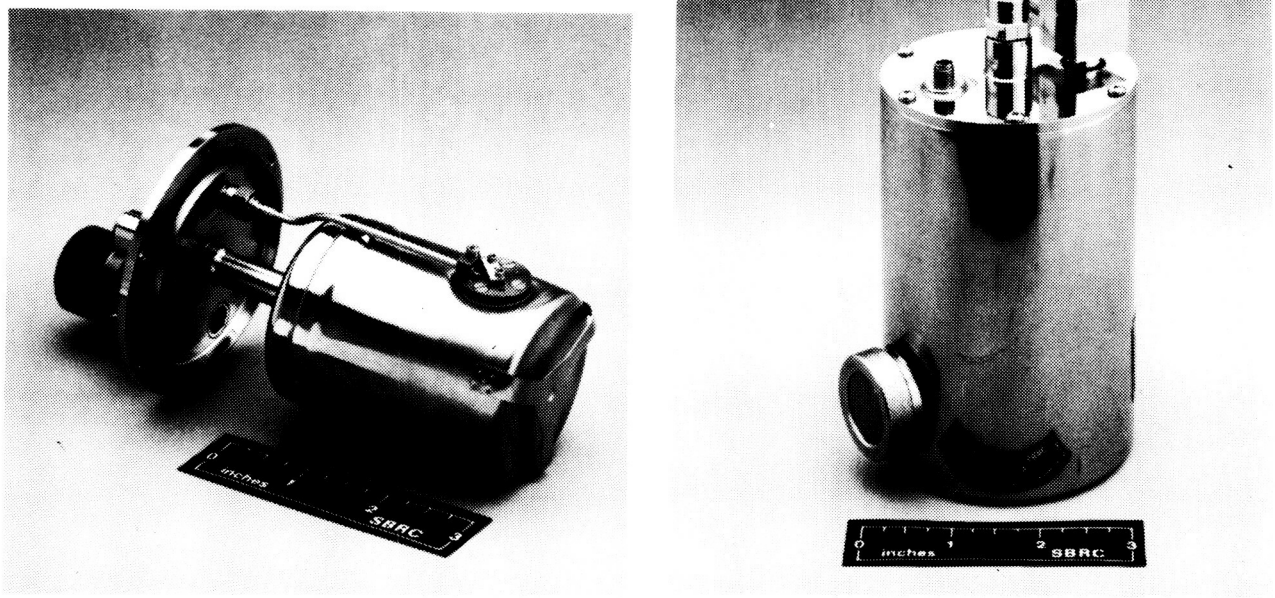

(A) Inner Assembly (B) External View

Figure 4-3. Photograph of Liquid Nitrogen Dewar Modified for High Frequency Photomixer Testing

4.2 PHOTOMIXER TESTING

To test photomixer diode performance, the following measurements were carried out:

1. DC current versus voltage
2. Low frequency blackbody detectivity
3. Relative spectral response versus wavelength
4. High frequency heterodyne signal versus frequency
5. High frequency noise versus frequency
6. Heterodyne noise equivalent power (NEP_H)

Procedures for the first three tests are well known and standardized throughout the industry and do not need to be described here. The heterodyne performance tests are not so well known so our test procedures are described below.

The heterodyne sensitivity in the GHz frequency range was tested using a blackbody technique whereby a CO_2 laser beam is mixed with blackbody radiation to produce the heterodyne IF signal.[12] During Phase I of this program, heterodyne sensitivity tests were performed at Hughes Aircraft Company's Space and Communications Division with a test set-up which has been previously described in the literature.[13] During Phase II of this program, the heterodyne sensitivity tests were performed at the Santa Barbara Research Center.

A block diagram of our test apparatus is shown in Figure 4-4. Figure 4-4(a) shows the optical lay-out. The chopped blackbody and laser LO beams are combined at a beam splitter and focused on the detector by a lens. The blackbody radiation is filtered by a narrow band-pass filter (0.4 μm) centered at 10.6 μm. The laser is a Linelite Laser Corporation Model 941 which is tunable with a PZT. The laser output line is continuously monitored by an Optical Engineering, Inc., CO_2 Spectrum Analyzer and all measurements are made using the P_{20} line at 10.5915 μm. A Brewster plate polarizer-attenuator permits convenient variation of the LO power over the range from 0.01 to 10 mW. The LO power is measured by a Laser Precision Corporation pyroelectric radiometer. A chopper in the laser beam is used when measuring the beam power with the radiometer and when aligning the LO beam on the detector. During detector heterodyne NEP measurements this chopper is turned off and a steady laser power is on the detector.

Figure 4-4(b) illustrates the signal processing employed to obtain a heterodyne NEP measurement. The detector is connected to a bias regulator circuit which provides constant-voltage bias and convenient read-outs of detector current and voltage. Various amplifiers were used depending on the frequency range to be covered. For the 0.1 to 1.5 GHz range we used a Miteq model AM-3A-000110 preamplifier followed by a Miteq model AM-4A-000110 post amplifier. This combination provided an overall gain of 84 dB, a bandwidth of 1.2 GHz and a noise figure of 2.0 dB at 0.5 GHz. For the 1 to 3 GHz range a B and H Model A3020 preamplifier was used followed by another B and H model A3020 plus an Avantek model 2X-A43-W7. This combination provided an overall gain of 58 dB, a bandwidth of 3 GHz and a noise figure of 3.7 dB at 1.0 GHz.

Following the detector and amplifier blocks are a Hewlett-Packard spectrum analyzer, a lock-in amplifier and x-y recorder. The spectrum analyzer has two plug-in modules. The model 8558B covered the frequency range from

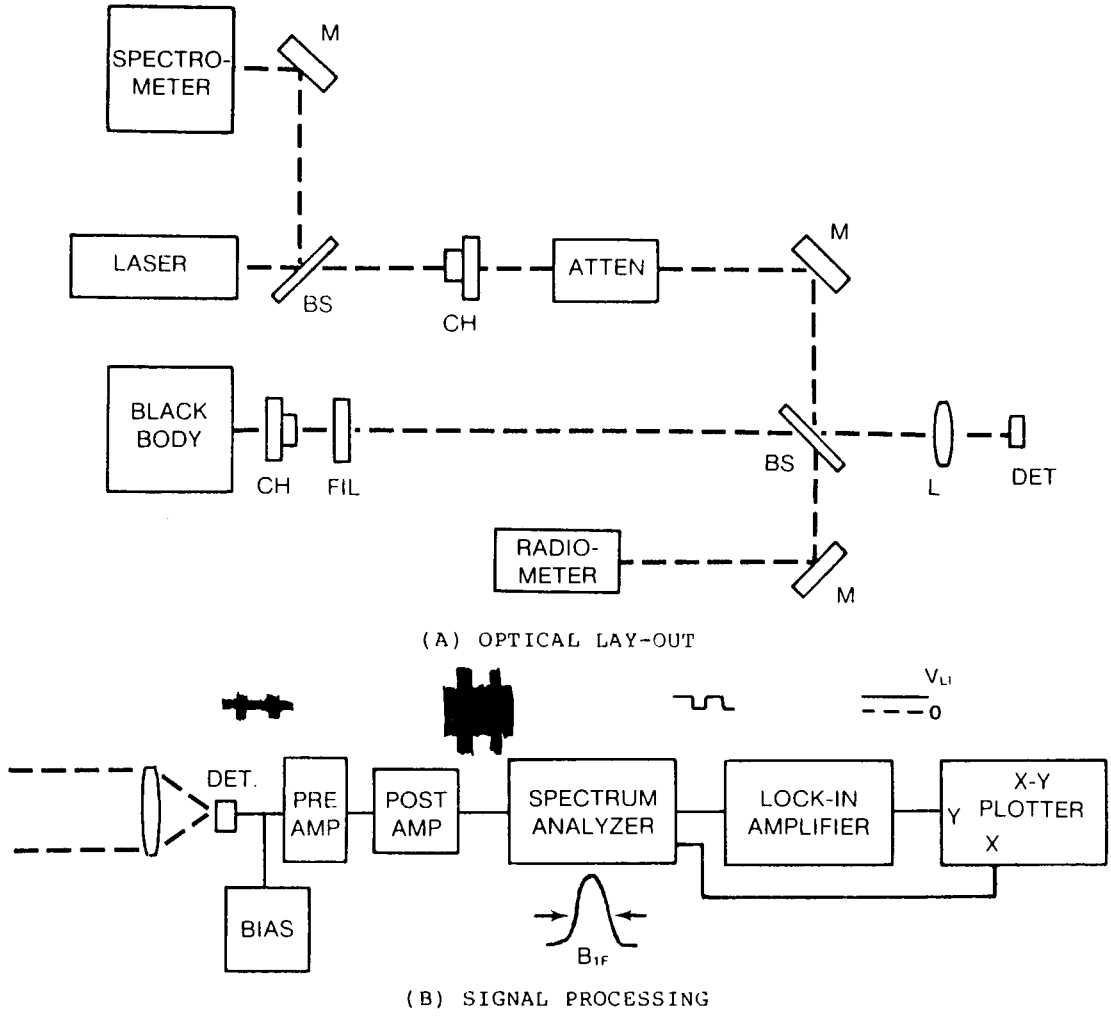

Figure 4-4. Block Diagrams for Blackbody Heterodyne NEP Testing

0.01 to 1.5 GHz and the model 8559A covered the range from 0.03 to 3 GHz. The spectrum analyzer bandwidth setting determines the IF bandwidth and the lock-in amplifier is required to extract the heterodyne signal from the noise because S/N ratios are less than unity with this measurement system. The output of the lock-in amplifier drives the y-axis of the recorder (signal amplitude) and the x-axis is driven by the frequency output from the spectrum analyzer. By selecting appropriate spectrum analyzer output terminals we could record swept frequency measurements of heterodyne signal, noise, and an output voltage related to the signal-to-noise ratio. The noise equivalent power is inversely proportional to S/N according to

$$NEP_H = \frac{P_s B}{(S/N)_{IF}} , \tag{31}$$

and, for heterodyne mixing with blackbody radiation, the signal power is given by

$$P_s = \frac{2h\nu B T_0}{\left[\exp\left(\frac{h\nu}{kT_B}\right) - 1\right] - \left[\exp\left(\frac{h\nu}{kT_A}\right) - 1\right]} , \tag{32}$$

where

$h\nu$ = photon energy

B = electrical noise bandwidth of spectrum analyzer

T_0 = transmission of optics

k = Boltzmann's constant

T_B = blackbody temperature

T_A = ambient temperature

therefore, the heterodyne NEP per unit bandwidth is

$$\frac{NEP_H}{B} = \frac{2h\nu T_0}{\left[\exp\left(\frac{h\nu}{kT_B}\right) - 1\right] - \left[\exp\left(\frac{h\nu}{kT_A}\right) - 1\right](S/N)_{IF}} \tag{33}$$

An ideal photomixer operating at the quantum limit has a heterodyne NEP

$$\frac{NEP_H}{B} = h\nu = 1.87 \times 10^{-20} \text{ W/Hz} \tag{34}$$

at 10.6 μm. By comparison of the real detector's NEP with this ideal detector one has the effective heterodyne quantum efficiency

$$\eta_H = \frac{1.87 \times 10^{-20}}{(NEP_H/B) \text{ measured}} . \tag{35}$$

This measured value of η_H may then be compared with the theoretically predicted value given previously by equation (29).

Section 5
TEST RESULTS

This program was carried out in two phases. Eight photomixers were fabricated and delivered during Phase I and eight more photomixers were fabricated and delivered on Phase II, one of these being mounted in an LN_2 dewar along with a cryogenic GaAs FET preamplifier circuit. The test results for all of these devices will be presented below by phase.

5.1 PHASE I RESULTS

Table 5-1 summarizes the low frequency, direct detection test data for the eight photomixers delivered on Phase I of this program. The various columns of this table give contract serial numbers, chip identification number, zero bias dynamic resistance R_0, current responsivity R_I, quantum efficiency η, detectivity D*, and wavelengths for peak response λ_p and cut-off λ_c (i.e., wavelength where relative response is down by 50% from the peak response).

Table 5-1. Summary of Low Frequency, Direct Detection Test Data for 8 Photomixers Delivered on Phase I

Serial No.	Chip I.D. No.	R_0 (Ω)	R_I (A/W)	η (%)	$D^*(\lambda_p, 2\ kHz)$ (cm $Hz^{1/2}/W$)	λ_p/λ_c (μm)
V224-01	ZH223-2F (5,10)	70	4.8	57	2.0×10^{10}	10.7/12.4
V224-02	V8-93 (1,5)	1,600	4.9	55	3.7×10^{9}	11.0/-
V224-03	V8-93 (1,7)	550	5.5	64	1.0×10^{10}	11.0/11.8
V224-04	V8-93 (3,3)	700	3.6	42	8.2×10^{9}	10.4/11.6
V224-05	V8-93 (3,4)	1,000	3.7	44	1.1×10^{10}	11.4/12.4
V224-06	V8-88 (2,1)	300	4.0	45	5.0×10^{9}	≈11/-
V224-07	V8-93 (1,1)	1,500	5.2	59	1.4×10^{10}	≈11/-
V224-08	V8-93 (1,9)	500	5.7	65	7.6×10^{9}	≈11/-

Sensitive Area = 1.53×10^{-4} cm^2
T = 77K.

A typical current-voltage curve for one of these diodes is shown in Figure 5-1. The zero bias dynamic resistance is obtained from the slope of the curve as it crosses V = 0 and for this example is found to be 1,500Ω. Another important parameter calculated from this curve is the series resistance which

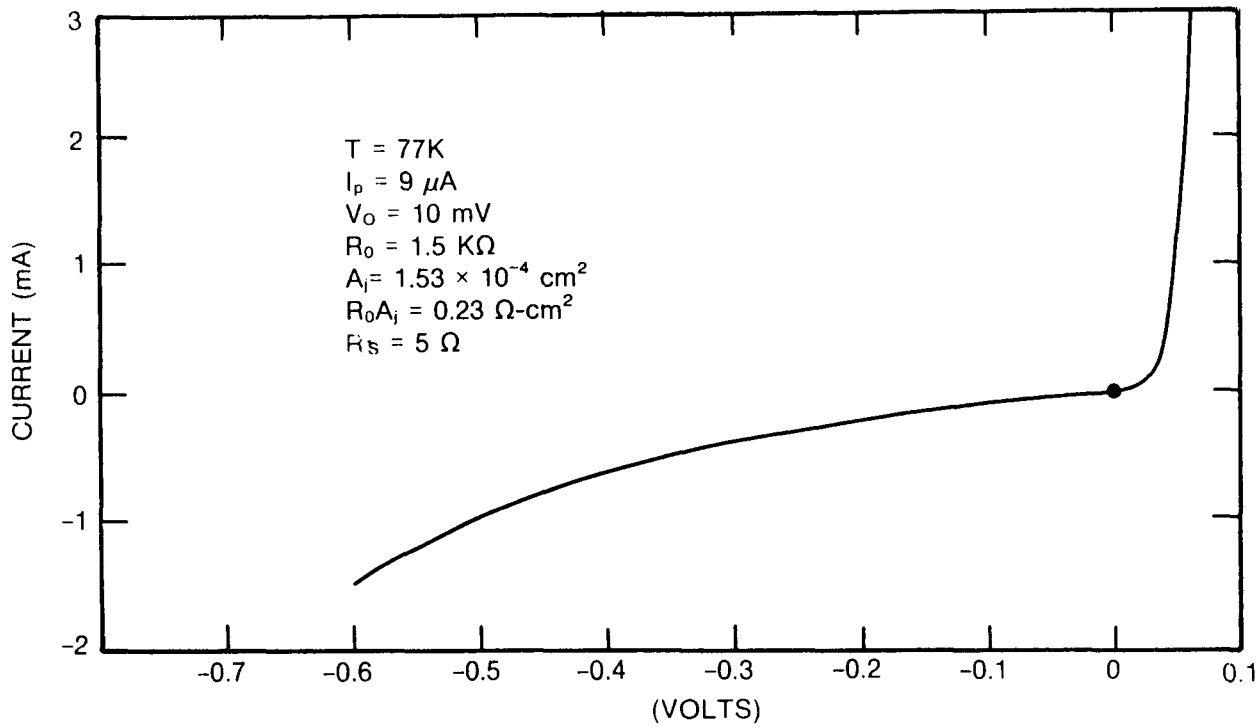

Figure 5-1. Current Versus Voltage Curve for Phase I Photomixer No. V224-07

is obtained from the slope at high forward bias. In this example we measured 5Ω. For high frequency photomixing, the diode is operated in reverse bias and we would like to keep the dark current less than 1 to 2 mA. Therefore, a bias voltage of 0.5 to 0.6V would be appropriate for this example and, in fact, we typically ran this devices at about 0.5V of reverse bias.

Figure 5-2 shows a typical relative spectral response curve. Also shown in this figure is a transmission spectrum for the epoxy resin used to bond the HgCdTe to the Irtran 2 substrate. This spectrum does not represent the absolute transmittance of the epoxy layer. It was acquired by bonding two flat Ge plates together with the epoxy and measuring the transmittance of the sandwich test structure. Reflection losses at the Ge surfaces have not been taken out. Additionally, the thickness of the epoxy layer in the test structure is somewhat greater than in the detector. The message that we are trying to convey with this data is that, in spite of a few strong IR absorption lines, the epoxy is reasonably clear in the 10 to 11.5 μm range as well as in the ranges 4 to 6 μm and 12.5 to 15 μm. The detector's relative spectral response data supports this conclusion. The general shape of this spectral response curve

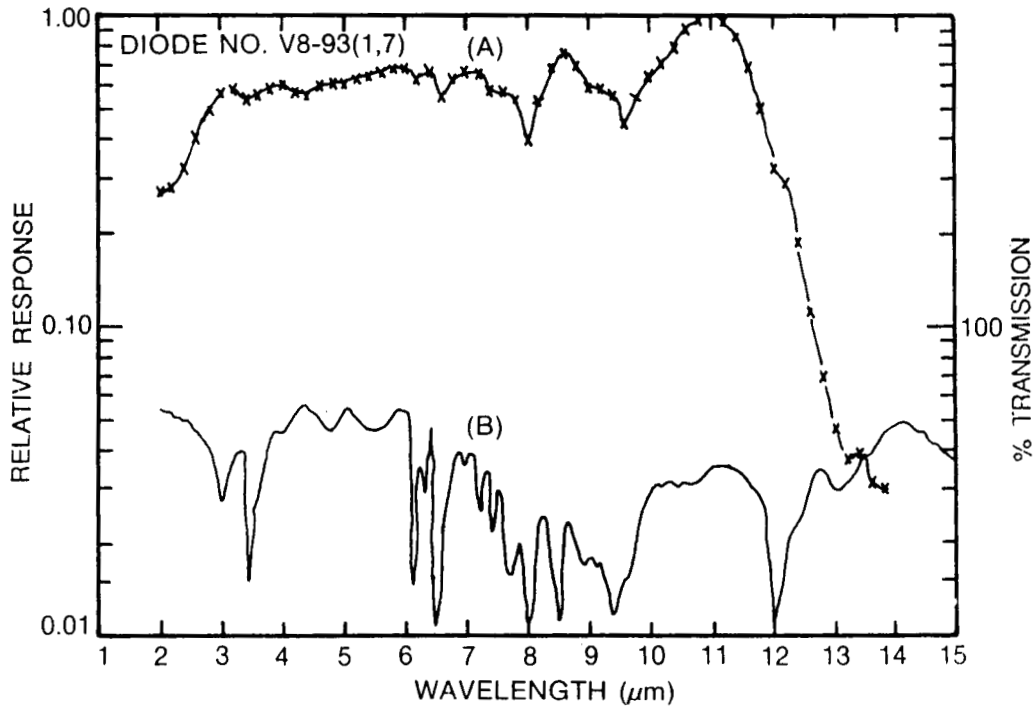

Figure 5-2. (a) Relative Spectral Response of Typical Phase I Photomixer; (b) Relative Transmission of Epoxy Resin Used to Bond HgCdTe to the Irtran 2 Substrate

is as expected for a quantum detector but with the addition of absorption dips at the strongest epoxy absorption lines, namely, 3.5, 6.5, 8.0, 9.5, and 12.0 μm. Absorption by the epoxy at our test wavelength of 10.6 μm is probably less than 10%.

Figure 5-3 shows the raw data plots of heterodyne signal and noise versus frequency for a typical Phase I photomixer, number V224-04. In Figure 5-3(a) the frequency range is 0.1 to 2 GHz and in Figure 5-3(b) the frequency range is 2 to 6 GHz. The ordinate is in negative dBs and the signal levels are on the order of 15 dB lower than the noise, indicating signal-to-noise ratios of about 0.03. The raw data was converted to effective heterodyne quantum efficiency and heterodyne NEP using the following formulas:

$$\eta_H = \frac{(S/N)_{IF}}{2T_0\left[\frac{1}{\exp\left(\frac{h\nu}{kT_B}\right) - 1} - \frac{1}{\exp\left(\frac{h\nu}{kT_A}\right) - 1}\right]}, \qquad (36a)$$

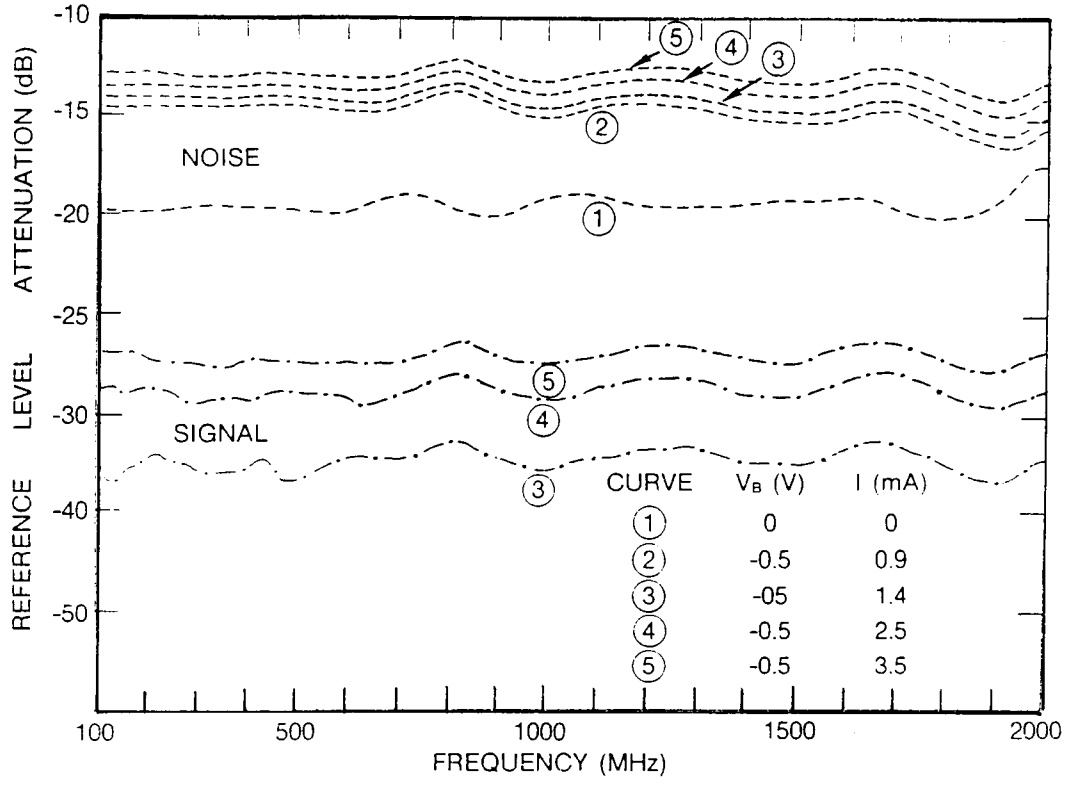

(A) 0.1 to 2 GHz Range

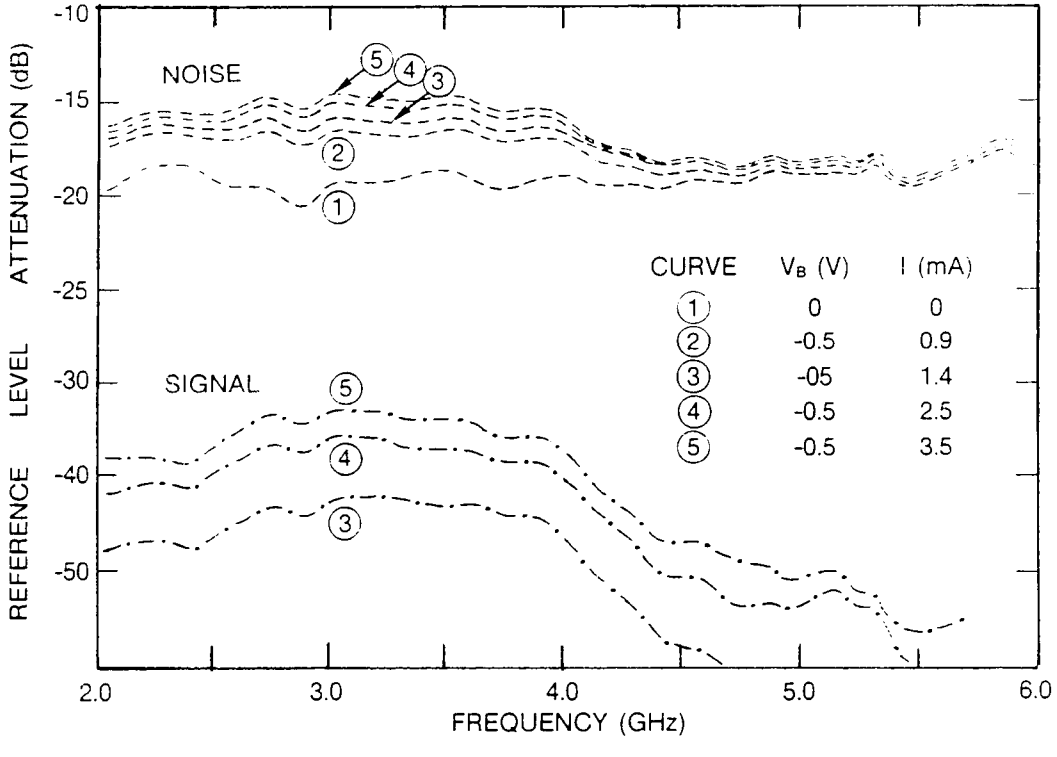

(B) 2.0 to 6.0 GHz Range

Figure 5-3. Output Data Records for Heterodyne Signal and Noise versus Frequency (Photomixer No. V224-04)

$$\eta_H = \frac{(S/N)_{IF}}{0.203} , \tag{36b}$$

$$\frac{NEP_H}{B} = \frac{h\nu}{\eta_H} = \frac{1.87 \times 10^{-20}}{\eta_H} , \tag{37}$$

where T_0 is the transmittance of optical components between the blackbody and photomixer (0.3), T_B is the blackbody temperature (1,006K), T_A is the ambient temperature (296K), and $h\nu$ is the photon energy for 10.6 μm radiation (1.87×10^{-20}J). Figure 5-4 shows a plot of heterodyne NEP_H/B and effective heterodyne quantum efficiency versus frequency derived from the raw data plots of Figure 5-3. This device has an NEP_H/B of 1.2×10^{-19} W/Hz which remains constant out to 1.2 GHz and then increases. The 3-dB frequency for NEP_H/B is seen to be 3.5 GHz. The η_H value is 16% in the lower frequency region. Additional data on the operating parameters for this photomixer (bias voltage, current, LO power, etc.) are listed in Figure 5-4.

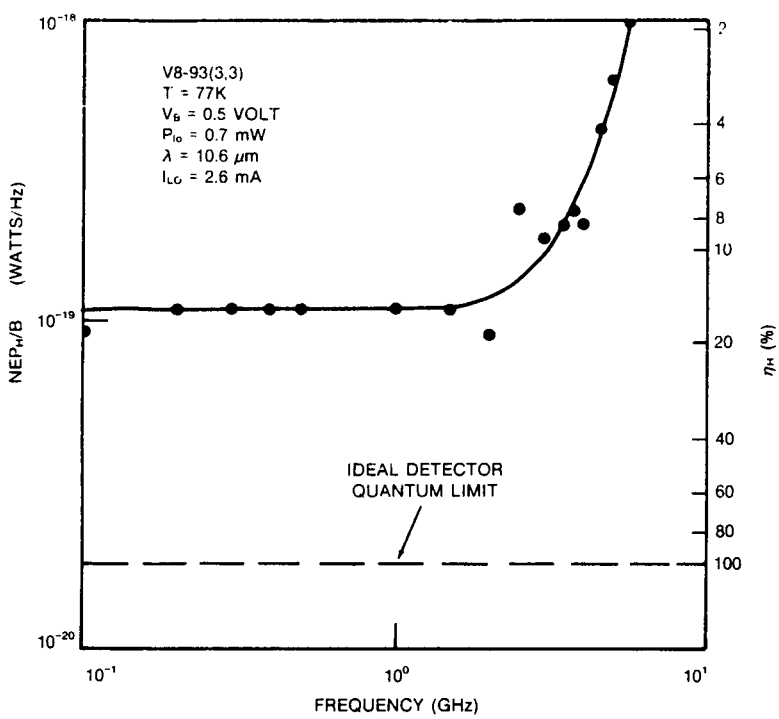

Figure 5-4. Noise Equivalent Power and Effective Heterodyne Quantum Efficiency Versus Frequency for Photomixer No. V224-04

It is also of interest to examine the frequency dependence of the heterodyne signal alone. Figure 5-5 shows a plot of data points calculated from the raw data for photomixer number V224-05. It is seen that the 3-dB frequency for the heterodyne signal is 1.6 MHz for this device. Additionally, we calculated theoretically the frequency response using the frequency function $F(\omega)$ given in equation (21). This frequency function was derived by assuming that the photomixer's high frequency roll-off is controlled by the capacitance and inductance of the photomixer plus its mount and connecting wires. To calculate $F(\omega)$, the measured values of R_d, R_ℓ and R_s for this detector were employed and the capacitance C and inductance L were used as adjustable parameters to obtain a "best fit" to the experimental data points. Values of C and L arrived at by this procedure were C = 1 pF and L = 4 nH. The theoretical data shown by the solid line in Figure 5-5 is in reasonably good agreement with the experimental data points. The capacitance value required is about as expected based on a p-n junction area of 1.5×10^{-4} cm^{-2} in the HgCdTe. The fit could be accomplished only by introducing a nonzero inductance value. The value arrived at, namely 4 nH, also seems reasonable based on the device geometry and connecting wires.

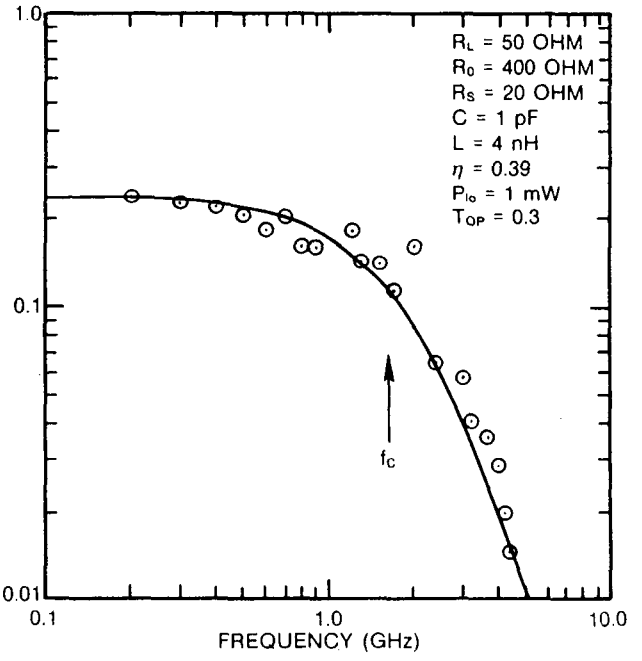

Figure 5-5. Relative Heterodyne Signal Versus Frequency for Photomixer No. V224-05 (V8-93 (3,4))

Figure 5-6 shows NEP_H/B versus frequency plots for all Phase I photomixers for which data was available. Also shown on the right hand axis is the heterodyne quantum efficiency. The best photomixers have a heterodyne quantum efficiency at 1 GHz of about 20%. The NEP_H bandwidth (i.e., the frequency where NEP_H/B has increased by a factor of 2) is at least 2 GHz for all of the photomixers and, for two of them, it was in the range 3 to 4 GHz.

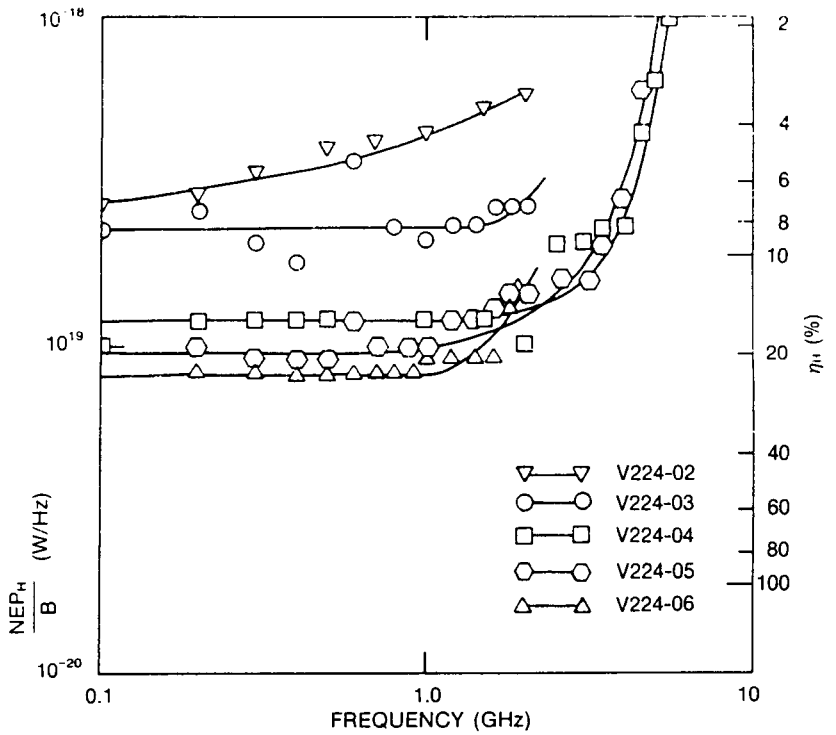

Figure 5-6. Heterodyne NEP Versus Frequency for Five Phase I Photomixers

Table 5-2 summarizes the operating conditions, NEP_H/B at 1 GHz, effective heterodyne quantum efficiency at 1 GHz, and the NEP bandwidth for 5 of the 8 photomixers delivered on Phase I. High frequency heterodyne measurements were not made on the other three detectors. These data show that, even though excellent bandwidth was achieved with these photomixers, the heterodyne NEP was considerably higher than the theoretical limit of 1.87×10^{-20} W/Hz. Based on our measured quantum efficiency which averaged 54% for the eight photomixers, better NEPs were expected. Analysis of the test data showed that a major cause for the poor NEP was the use of a preamplifier with fairly high noise (The effective noise temperature of the preamplifier was reported to be ≈1000K). Secondary causes of poor NEP were high dark current noise and

Table 5-2. Heterodyne Sensitivity Data for 5 Photomixers Delivered on Phase I.

Serial No.	Chip I.D. No.	Bias (V)	I_D (mA)	I_{LO} (mA)	PLO (mW)	NEP_H/B @1GHz (W/Hz)	η_H @1GHz (%)	NEP BW (GHz)
V224-02	V8-93(1,5)	0.6	1.0	2.7	0.6	4.4×10^{-19}	6	2
V224-03	V8-93(1,7)	0.65	--	--	0.5	2.3×10^{-19}	8	>2
V224-04	V8-93(3,3)	0.5	0.9	2.6	0.7	1.2×10^{-19}	16	4
V224-05	V8-93(3,4)	0.6	1.2	1.6	0.5	9.5×10^{-20}	20	3
V224-06	V8-88(2,1)	0.6	2.5	--	0.6	8.0×10^{-20}	23	2

quantum efficiency of only 54%. For the Phase II effort, a major goal was to reduce preamplifier noise by use of a cryogenic GaAs FET preamplifier. Additionally, we sought to reduce dark current by improving the p-n junction formation technique and to increase quantum efficiency by the use of antireflection coatings.

5.2 PHASE II TEST RESULTS

Table 5-3 summarizes the low frequency, direct detection test data for the eight photomixers delivered on Phase II of this program. Detectivity data was not measured on any of these devices. The main thing to be noticed in this table is improvement in quantum efficiency over the Phase I photomixers. The average here was 58% and, if the one poor device (No. V224-09) which peaked at too short a wavelength is eliminated, the average becomes 62%. This improvement in quantum efficiency was obtained by using a ZnS antireflection coating on the backside of the HgCdTe material where radiation enters after passing through the Irtran 2 substrate. Additional improvement in quantum efficiency could be obtained by coating the surfaces of the substrate, but this has not yet been attempted.

The high frequency heterodyne sensitivity test data for the Phase II photomixers is summarized in Table 5-4. The operating characteristics of these devices in term of bias voltage, dark current, and local oscillator power are quite similar to the Phase I photomixers as are the heterodyne NEP and effective heterodyne quantum efficiency values. One exception is device number

Table 5-3. Summary of Low Frequency, Direct Detection Test Data for 8 Photomixers Delivered on Phase II.

Serial No.	Chip I.D. No.	R_I (A/W)	η (%)	λ_p/λ_c (μm)
V224-09	V850-1EA(3,2)	2.9	34	9.0/11.3
V224-10	V850-1EA(3,4)	5.2	61	10/11.2
V224-11	V850-1EA(2,4)	5.7	67	--
V224-12	V850-1CB(6,1)	7.2	84	--
V224-13	V850-1CB(5,4)	5.9	69	--
V224-14	V850-1EA(2,5)	5.2	61	10/11.4
V224-15	V573-1DA(3,7)	3.2	38	11/12
V224-16	V573-1DA(3,6)	4.5	53	11/12

Sensitive Area = 1.53×10^{-4} cm2
T = 77K

V224-16 which had an exceptionally good heterodyne NEP value of 5.3×10^{-20} W/Hz at 1 GHz. The reason for the good performance of this photomixer was that it had a strong heterodyne signal even beyond 1 GHz whereas the other devices exhibited a heterodyne signal which rolled off before 1 GHz resulting in poor signal-to-noise ratio at the higher frequencies. We believe that this was due to a wider depletion region in this device because of a lower net donor concentration in the region of the wafer from which the photomixer was made. The second best device, No. V224-15, also came from the same region of that wafer. The other devices were fabricated from other wafers which probably had higher donor concentration resulting in a narrow depletion layer which did not extend throughout the whole thickness of the HgCdTe layers. Thus slow moving holes created outside the depletion layer could not be efficiently collected at high frequencies and this resulted in loss of high frequency signal.

5.3 DETECTOR-COLD PREAMPLIFIER ASSEMBLY

The best photomixer fabricated for Phase II was selected for mounting in a dewar housing along with a cold GaAs FET preamplifier. Figure 5-7 and 5-8 show photographs of the detector/cold preamplifier assembly. In this section

Table 5-4. Heterodyne Sensitivity Data for 8 Photomixers Delivered on Phase II.

Serial No.	Chip I.D. No.	Bias (V)	I_D (mA)	I_{LO} (mA)	PLO (mW)	NEP_H/B @1GHz (W/Hz)	η_H @1GHz (%)	BW(NEP) (GHz)
V224-09	V850-1EA(3,2)	0.16	0.51	1.9	0.65	1.4×10^{-19}	13	>1.5
V224-10	V850-1EA(3,4)	0.30	0.55	1.5	0.28	1.3×10^{-19}	15	>1.5
V224-11	V850-1ES(2,4)	0.39	1.27	3.1	0.70	2.1×10^{-19}	9	>1.5
V224-12	V850-1CB(6,1)	0.25	0.40	8.3	1.16	2.4×10^{-19}	8	>1.5
V224-13	V850-1CB(5,4)	0.39	5.80	4.1	0.69	4.4×10^{-19}	4	--
V224-14	V850-1EA(2,5)	0.30	0.67	3.8	0.72	1.4×10^{-19}	13	>1.5
V224-15	V573-1DA(3,7)	0.40	5.5	3.8	1.20	9.1×10^{-20}	20	2
V224-16	V573-1DA(3,6)	0.42	3.6	9.4	2.10	5.3×10^{-20}	35	2

T = 77K

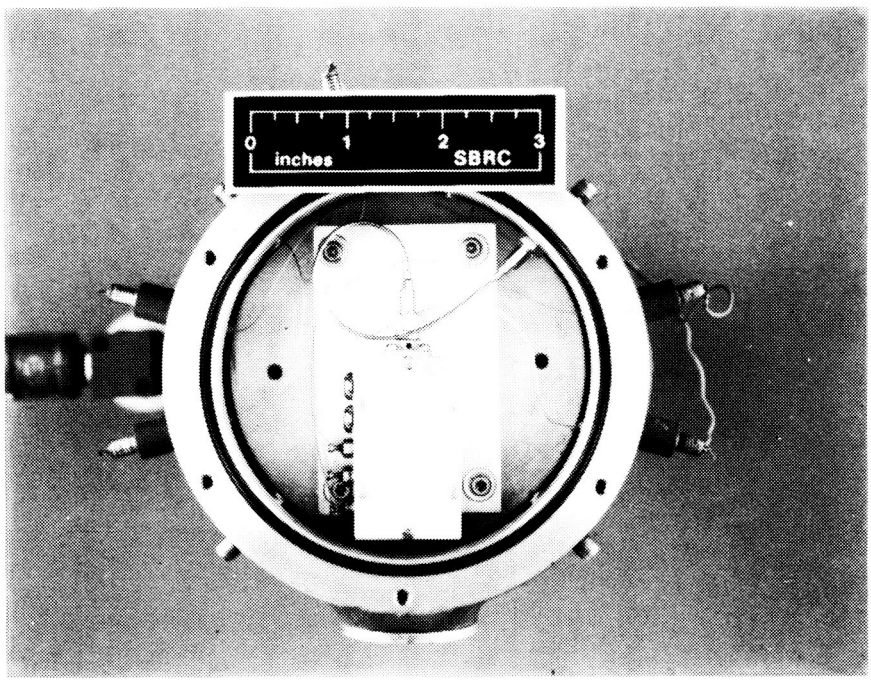

Figure 5-7. Photograph of Detector/Cold GaAs FET Preamp Housing Attached to Dewar Cold Plate. (Bottom Cover of Dewar Removed.)

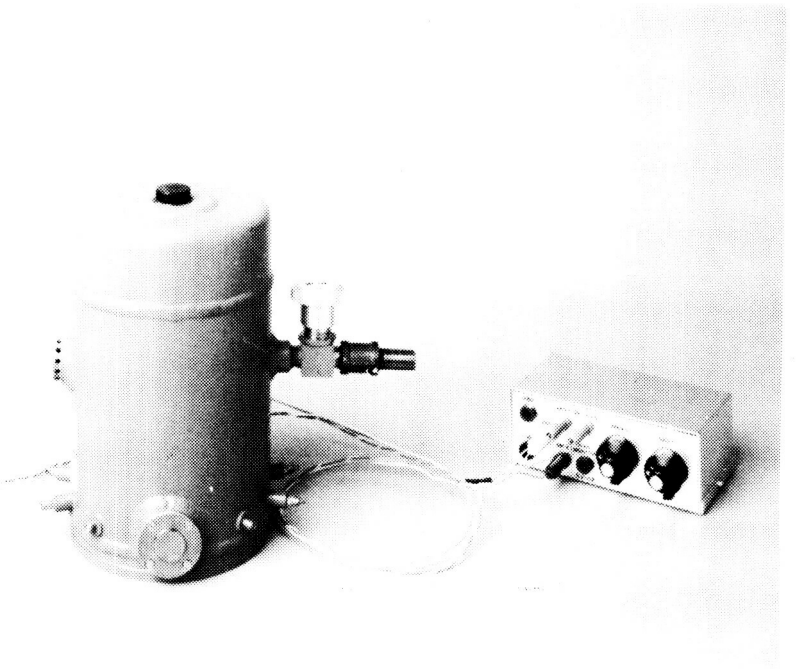

Figure 5-8. Photograph of Dewar Assembly and Bias Box with Wire Leads Attached

we describe the dewar design as well as the electronic circuits, and present the test results.

5.3.1 Dewar Design

The LN_2 dewar was a Cryogenics Associates Model IR212 specially constructed for this program. It had a one-liter liquid coolant capacity which provided a hold time for the LN_2 in excess of 24 hours. A 4-inch diameter cold plate provided ample space for mounting the detector and cold preamplifier assembly. The cold plate was rigidly connected to the dewar bottom flange by an epoxy-fiberglass cylinder. This prevented any motion of the cold plate with respect to the dewar outer wall and thus prohibited optical microphonics due to vibration of the detector-preamplifier assembly with respect to the laser beam.

The dewar had a side-looking window which was antireflection coated ZnSe purchased from II-VI Incorporated. Test data furnished by the vendor indicated a transmittance value of 98% at 10.6 μm.

A number of electrical feed-throughs were provided in the dewar side wall. Four of these were SMA type 50 ohm coaxial feed-throughs. Five were L-C low-pass RF suppression type feed-throughs for dc bias connections. Only one coaxial feed-through and three RF suppression feed-throughs were employed in the final assembly. A sturdy ground connection to the dewar wall was also provided in the form of an 8-32 stud.

5.3.2 Preamplifier Circuits

The cold preamplifier circuit was designed around an Avantek Model AT8110 low noise GaAs MESFET. This device has optimum gain and noise characteristics in the 1 to 3 GHz frequency range. Figure 5-9 shows the circuit diagram for all components located within the dewar. Additional circuits for setting the dc bias levels at drain, gate, and detector were located outside the dewar. Figures 5-10, 5-11, and 5-12 show these circuit diagrams. As seen from Figure 5-9, the preamplifier is a simple common-source circuit with voltage feedback for stabilization. Only one gain stage was incorporated in the initial design, however, space was left on the circuit board for an additional stage if desired at some future time.

Testing of the preamplifier circuit was initially performed without a detector connected to establish the optimum preamplifier bias control settings for best gain and noise figure. The nominal results from this testing are given in Table 5-5. On cooling to 77K, little change was observed in these characteristics. The gain dropped by about 1 dB and noise figure remained unchanged. This was a little surprising since it was expected that the noise would decrease with cooling. The reason this did not occur is not presently known.

Table 5-5. Nominal Operating Characteristics of Preamplifier at Room Temperature Without Detector Connected.

V_{DS} = 2.5 volt
V_{GS} = -0.3 volt
I_{DS} = 45 mA
Gain = 12 dB @ 1 GHz
NF = 3.1 dB @ 1 GHz
Bandwidth > 3 GHz

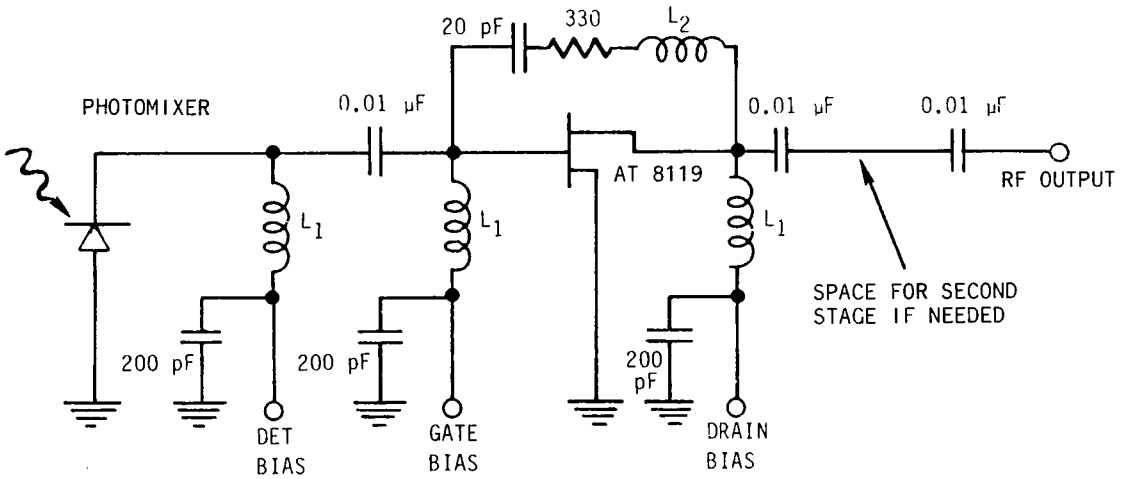

L_1 = 10 TURNS OF 0.010 INCH DIAMETER PHOSPHOR BRONZE WIRE

L_2 = SMALL LENGTH OF BRASS SHIM STOCK

CAPACITANCE VALUES LISTED ARE AT 300 K.
THESE DECREASE WHEN PREAMP IS COOLED TO ~77K.

Figure 5-9. Cooled GaAs FET Preamp Circuit

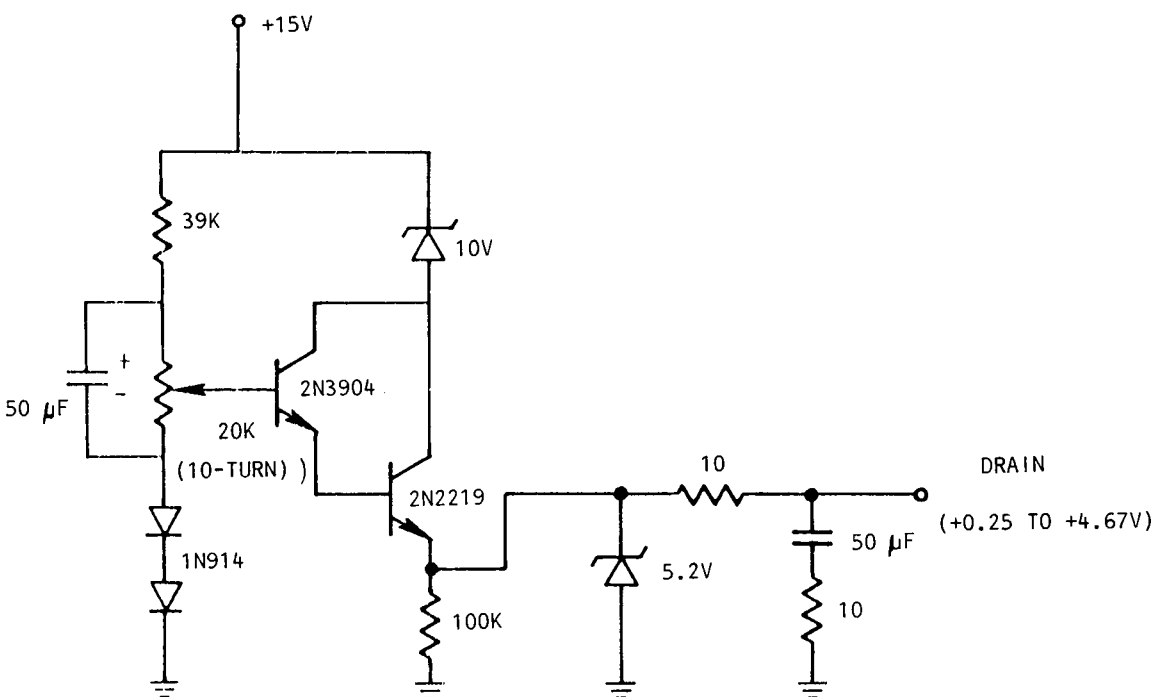

Figure 5-10. Drain Bias Control Circuit

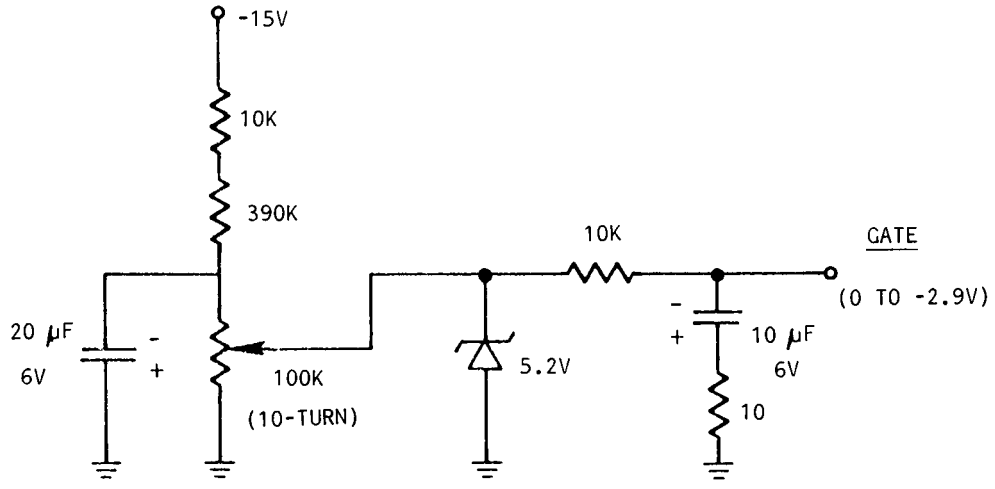

Figure 5-11. Gate Bias Control Circuit

5.3.3 Detector-Preamplifier Test Results

After preliminary testing of the photomixer detector and the cold preamplifier by themselves, the detector was assembled into the preamplifier housing and final testing was performed. Figure 5-13 shows schematically the set-up employed during these tests. The RF output from the preamplifier was sent to a post amplifier and then to a spectrum analyzer. Heterodyne sensitivity measurements were performed as a function of frequency and local oscillator power using the equipment previously described in Section 4.2.

Figures 5-14, 5-15, and 5-16 show the measured frequency dependence of the signal, noise, and NEP in the 0.1 to 1.5 GHz range. A sharp structure can be seen at 470 MHz which is very evident in both the signal and noise versus frequency plots (Figures 5-14 and 5-15). This is due to a resonance in the cold GaAs FET preamp circuit. Additionally, there are broad oscillations in the signal and noise curves which are due to VSWR. However, the NEP versus frequency curves are quite flat (Figure 5-16) because the oscillations are of the same magnitude in both the signal and noise, and NEP is inversely proportional to signal-to-noise ratio. Signal, noise and NEP curves were all taken

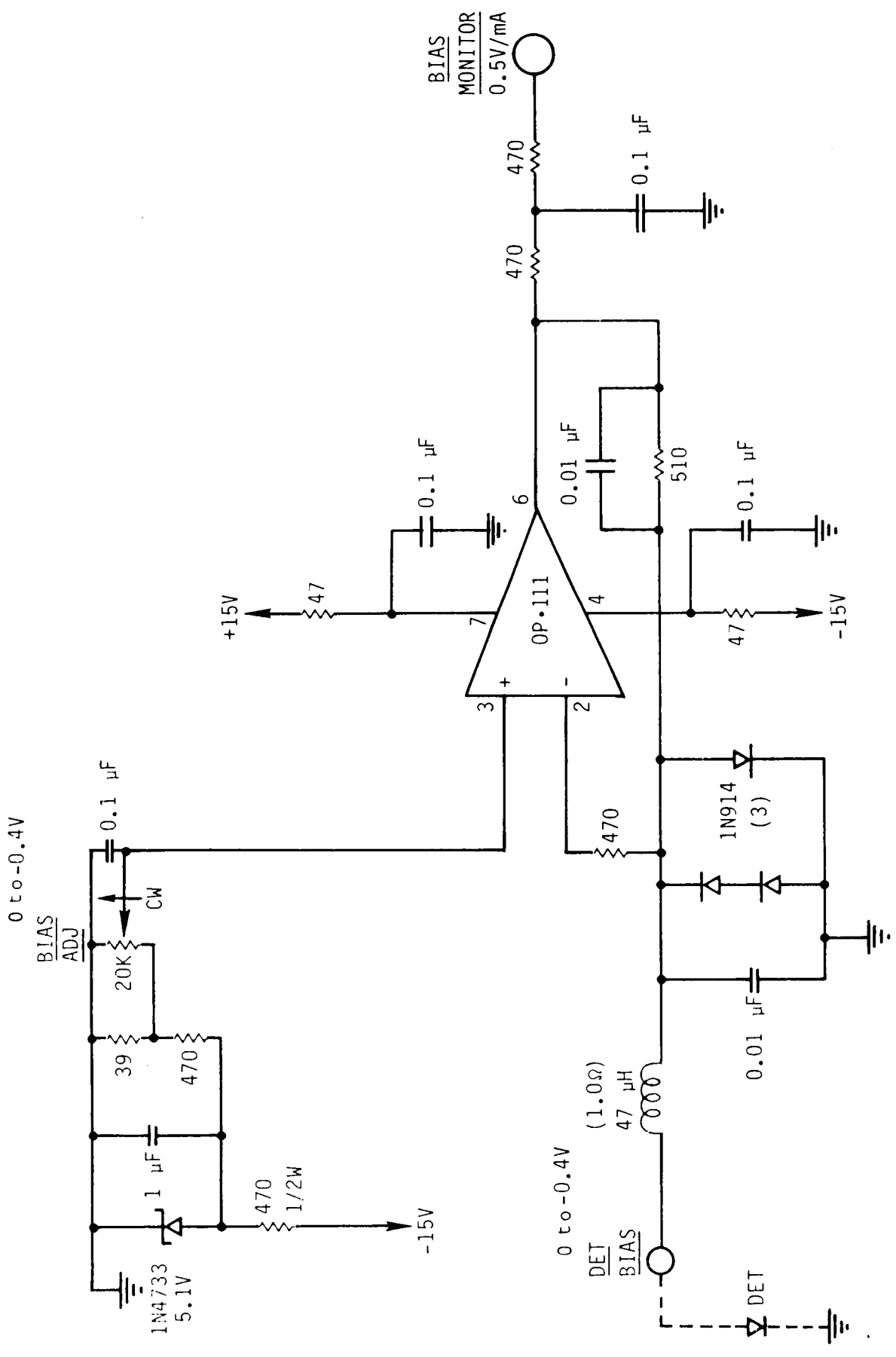

Figure 5-12. Detector Bias Control Circuit

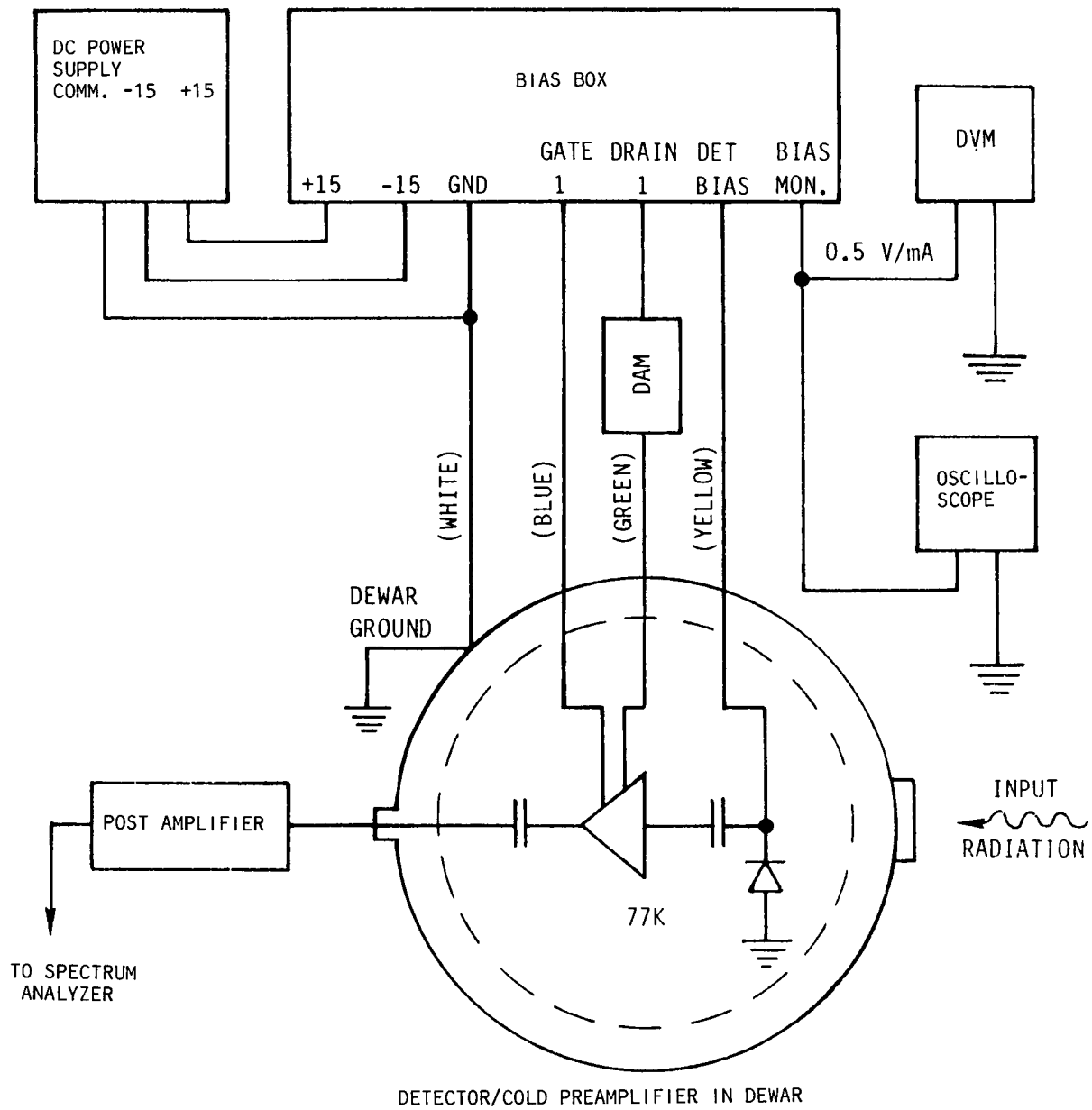

Figure 5-13. Wiring Diagram for Operation of Photomixer Detector and Cold Preamp

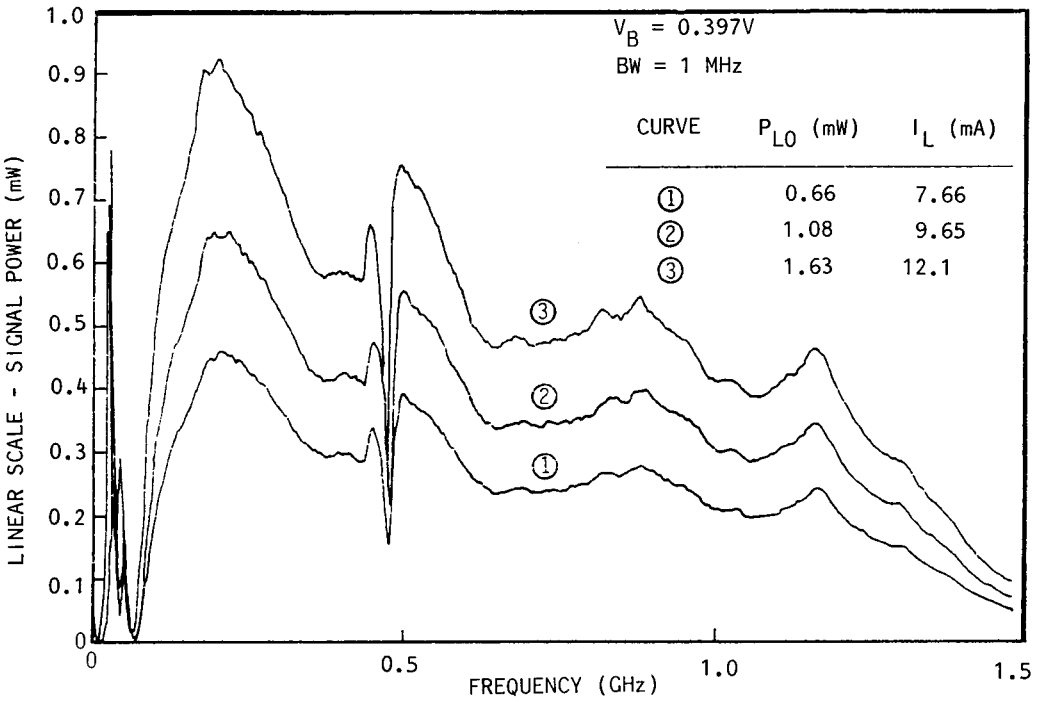

Figure 5-14. Signal versus Frequency, 1-1.5 GHz, Cold GaAs FET Preamp 3 GHz Post Amps, 8558 B Spectrum Analyzer

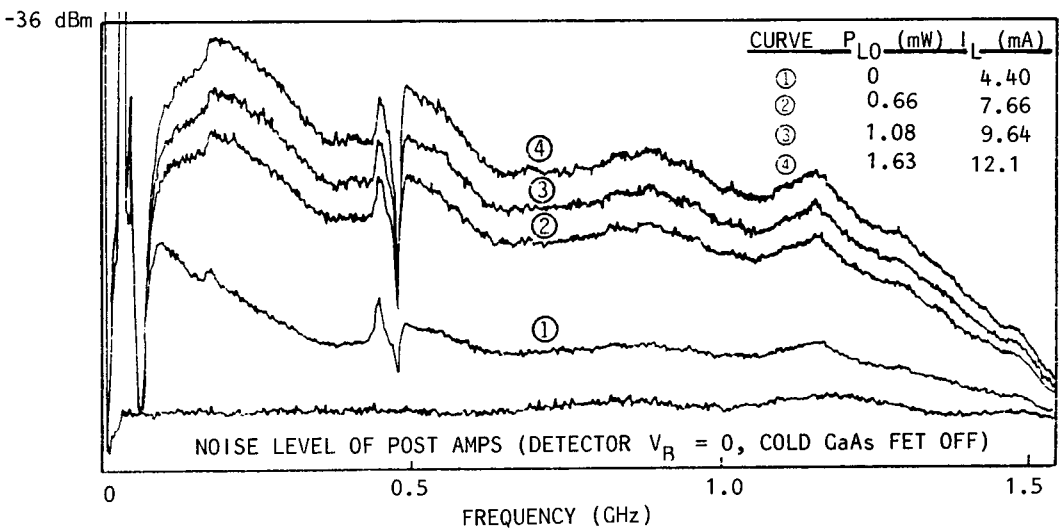

Figure 5-15. Noise versus Frequency, 1-1.5 GHz, Cold GaAs FET Preamp 3 GHz Post Amps, 8558 B Spectrum Analyzer

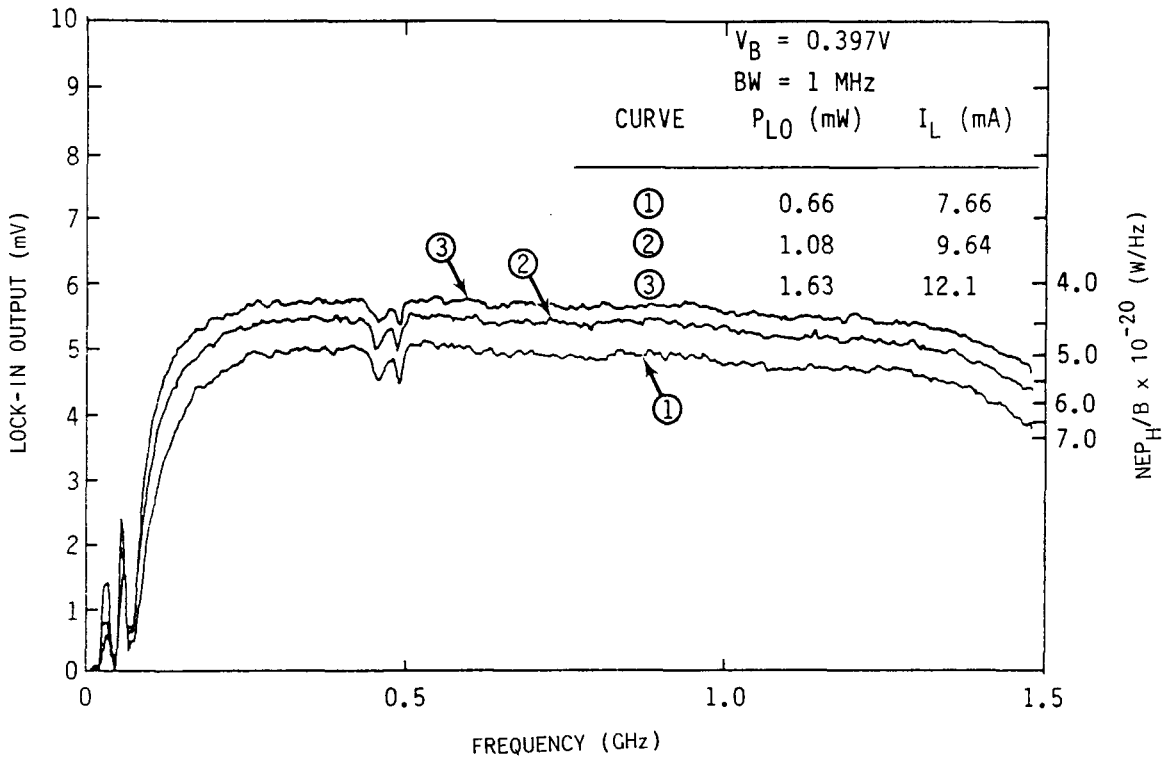

Figure 5-16. NEP versus Frequency, 1-1.5 GHz, Cold GaAs FET Preamp 3 GHz Post Amps, 8558 B Spectrum Analyzer

at a constant bias voltage of 0.397V but with different amounts of LO power on the photomixer. Note that NEP/B values less than 4.5×10^{-20} W/Hz are obtained out to 1.3 GHz at a P_{LO} value of 1.63 mW and diode current of 12.1 mA. Larger amounts of P_{LO} were not attempted in our tests because of concern for driving excessive current through the photomixer. We do not know at this time what the damage threshold is for these devices other than some current greater than 10 mA.

Figures 5-17, 5-18, and 5-19 show the measured frequency dependence of signal, noise, and NEP in the 0.1 to 3.0 GHz range. The structure in the 0.1 to 1.5 GHz region is similar to that shown in Figures 5-14, 5-15, and 5-16. There are additional dips in the 1.5 to 3.0 GHz range which are also due to the cold GaAs FET preamp circuit. A small peaking at 2.6 GHz is due to the post amplifiers.

Using smoothed NEP data from Figures 5-16 and 5-19 a plot of optimum NEP versus frequency was constructed on a log-log scale and this is shown in Figure 5-20. There is a slight difference in NEP values between the 0-1.5 and 0-3 GHz spectrum analyzers. The reason for this is not presently known. The key result of this plot shows that the 3-dB point for heterodyne NEP is 2 GHz.

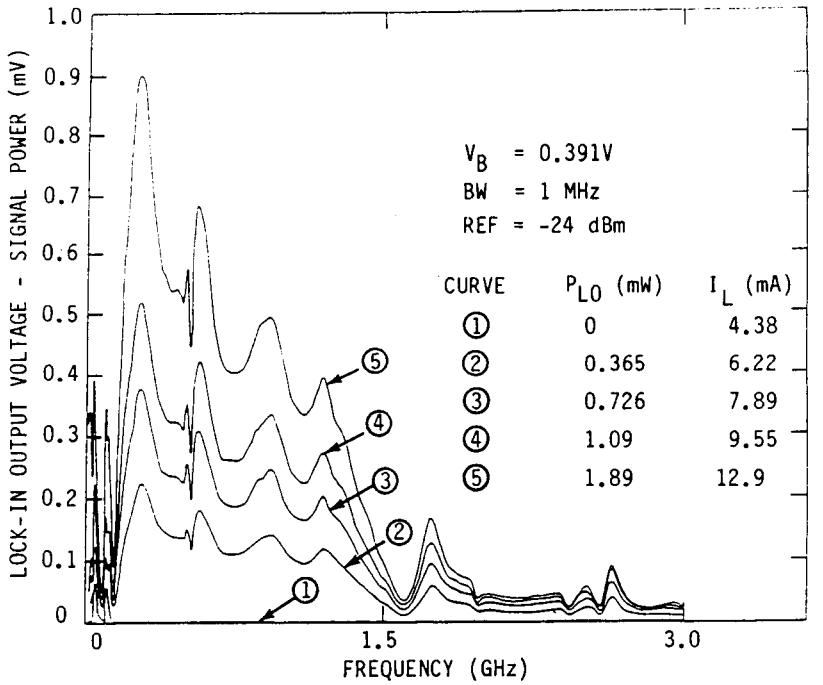

Figure 5-17. Signal versus Frequency, 0-3 GHz, Range Cold GaAs FET Preamp, 3 GHz Post Amps, 8559 A Spectrum Analyzer

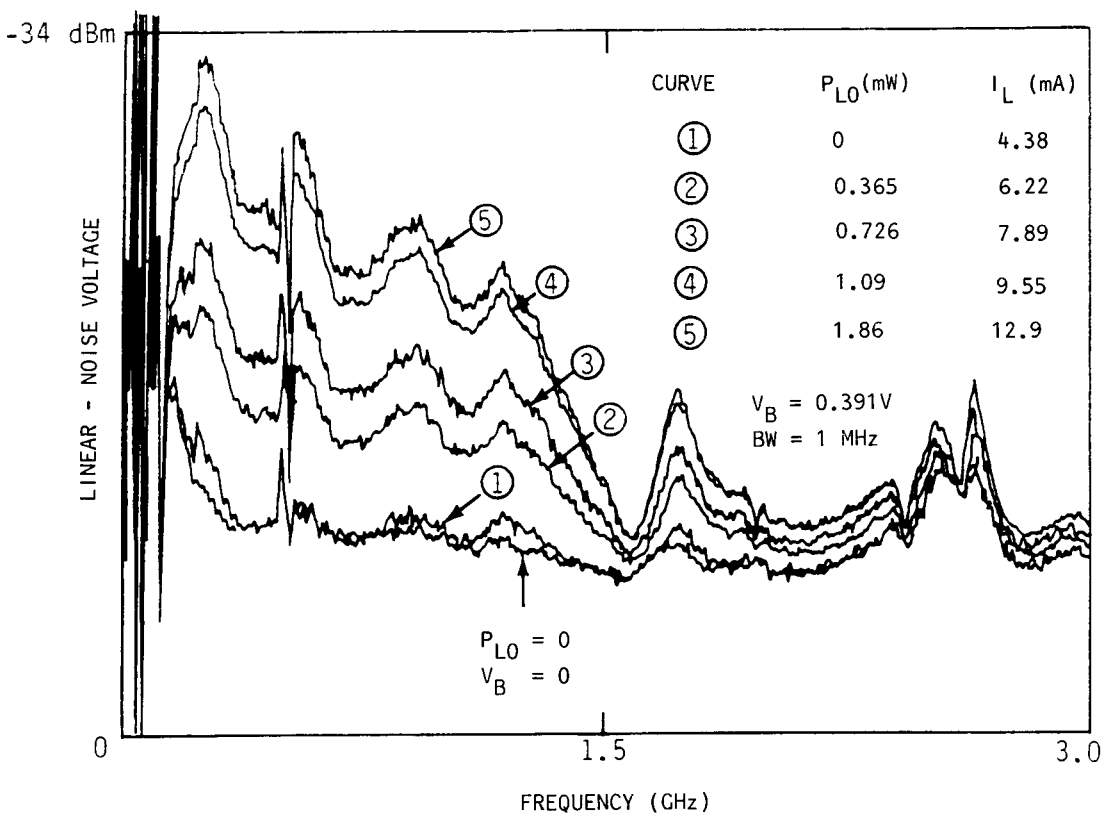

Figure 5-18. Noise versus Frequency, 0-3 GHz Range, Cold GaAs FET Preamp 3 GHz Post Amps, 8559 A Spectrum Analyzer

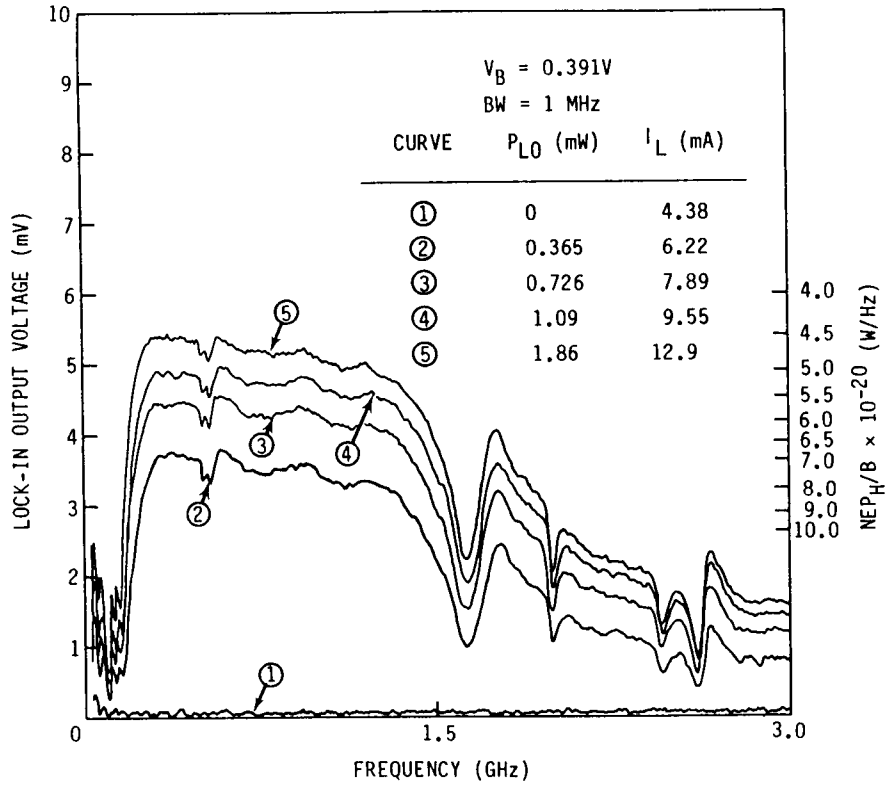

Figure 5-19. NEP versus Frequency, 0-3 GHz Range, Cold GaAs FET Preamp 3 GHz Post Amps 8559 A Spectrum Analyzer

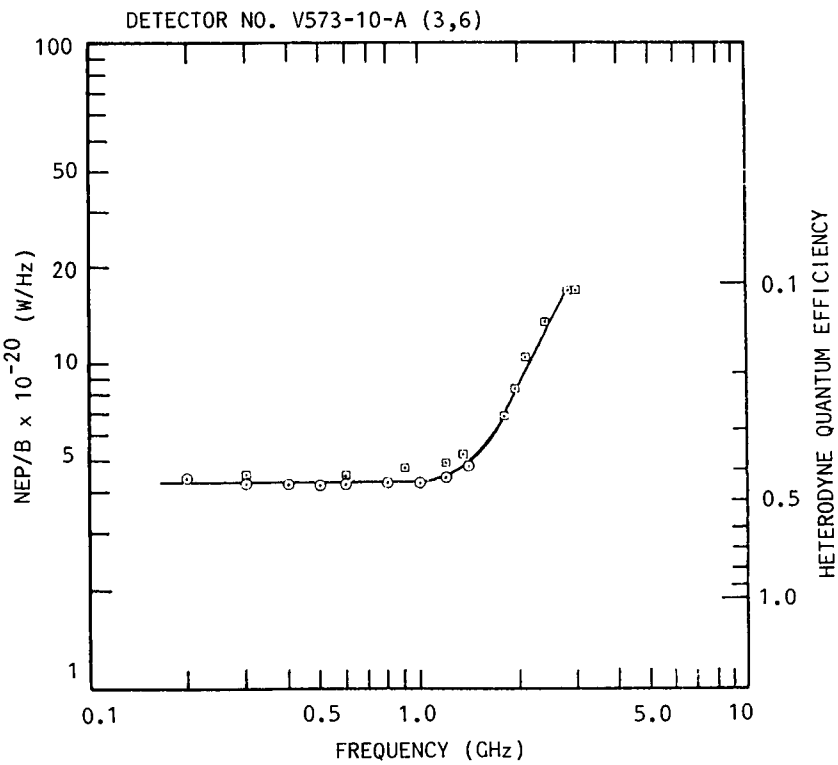

Figure 5-20. Heterodyne NEP versus Frequency

Section 6
CONCLUSIONS

The best photomixers made on Phase I had effective heterodyne quantum efficiencies of about 20%. This was less than the goal of 30%. However, these devices had bandwidths extending to 3-4 GHz which exceeded the Phase I goal of 2.0 GHz. The best photomixer made on Phase II had improved heterodyne quantum efficiency reaching a value of 44% as compared to the goal of 50%. Its bandwidth was 2.0 GHz compared to the goal of 2.5 GHz for Phase II.

This work has shown that high bandwidth and good heterodyne quantum efficiency can be obtained with the backside illuminated thin mesa diode structure. However, we have not yet demonstrated both of these qualities together in the same device. Additionally, the yield of high performance devices has been poor. Further work on the device fabrication technology is required to identify the problem areas. A good surface passivation technique also needs developing to assure the long term stability of completed photomixers.

Section 7
ACKNOWLEDGMENTS

Many people contributed to the work accomplished in this program. In particular, we would like to acknowledge the help of R.A. Cole for HgCdTe material preparation; K.M. Bushnell, J. Bettman, and R.L. Stallings for device fabrication; K.T. Gorton and C. Huang for testing at SBRC; and E.R. Brown who performed the Phase I heterodyne testing at Hughes Aircraft Co and also designed and built the cold GaAs FET preamplifier circuit.

We also gratefully acknowledge the support and encouragement of the program technical monitors at NASA Langley Research Center, H.D. Hendricks and W. E. Miller.

Section 8

REFERENCES

1. S.C. Cohen: Heterodyne Detection: Phase Front Alignment, Beam Spot Size, and Detector Uniformity, Appl. Optics 14, 1953 (1975).

2. R.H. Kingston: Detection of Optical and Infrared Radiation, Vol. 10, Springer Series in Optical Sciences, Springer-Verlag, New York, p. 26 (1978).

3. D.E. Sawyer and R.H. Rediker: Narrow Base Germanium Photodiodes, Proc. IRE 46, 1122 (1958).

4. W.W. Gartner: Depletion-Layer Photoeffects in Semiconductors, Phys. Rev. 116, 84 (1959).

5. A.S. Grove: Physics and Technology of Semiconductor Devices, J. Wiley and Sons, New York, Chapter 6 (1967).

6. D.L. Spears; T.C. Harman; I. Melngailis; and C. Freed: Solid State Research Report 1973:2. ESD-TR-73-100, MIT, May 15, 1973, p. 2.

7. D.L. Spears; T.C. Harman; and I. Melngailis: Solid State Research Report 1974:4. ESD-TR-74-328, MIT, Jan. 10, 1975. p. 5.

8. D.L. Spears: Planar HgCdTe Quadrantal Heterodyne Arrays with GHz Response at 10.6 μm, Infrared Physics 17, 5 (1977).

9. J.F. Shanley; T. Koehler; K. Lang; D. MacDonald; and B.J. Peyton: 10.6 Micrometer (Hg,Cd)Te Mixer/Detector Development: A Wideband Heterodyne Ladar Receiver, Contract No. DASG60-75-C-0079, Honeywell Radiation Center, 1977. (Available from DTIC as AD B020165L.)

10. J.F. Shanley; and C.T. Flanagan: N-P (Hg,Cd)Te Photodiodes for 8-14 Micrometer Heterodyne Applications, NASA Conference Publication 2138, Heterodyne Systems and Technology, Part II, p. 263, 1980.

11. C. Verie; and M. Sirieux: GHz Cutoff Frequency Capabilities of HgCdTe Photovoltaic Detectors at 10.6 μm, IEEE J. Quantum Elect. QE-8, 180 (1972).

12. D.L. Spears; and C.D. Hoyt: Solid State Research Report, 1978:1. ESD-TR-78-27, MIT, Feb. 15, 1978, p. 1.

13. E.R. Brown: Blackbody Heterodyne Receiver for NEP Measurements and Wideband Photodetector Characterization, Applied Optics, 21, 3602 (1982).

Section 9
APPENDICES

Appendix A

PHOTODIODE HIGH FREQUENCY CIRCUIT ANALYSIS

Figure A-1 shows the generally accepted high frequency equivalent circuit for a photodiode connected to a load R_ℓ. The photodiode can be considered as a current source in parallel with the diode ac resistance R_d and capacitance C. Also included in this circuit are the diode series resistance R_s and an inductance L which arises primarily from the lead wires.

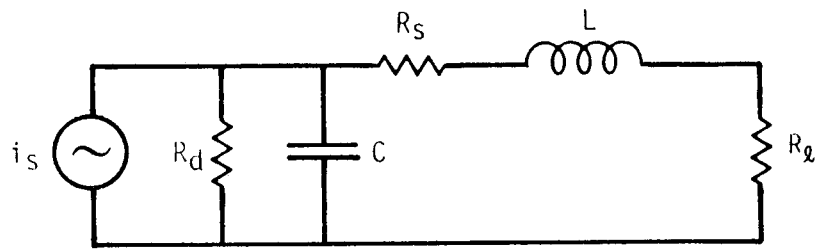

Figure A-1. High Frequency Equivalent circuit for a Photodiode Connected to a Load

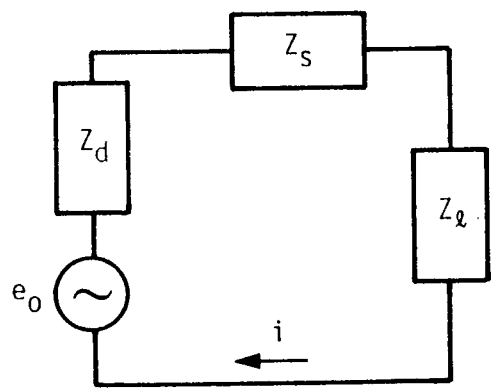

$$Z_d = \frac{R_d}{1 + jwCR_d}$$

$$Z_S = R_S + jwL$$

$$Z_\ell = R_\ell$$

$$E_o = i_S Z_d$$

Figure A-2. Thevenin Equivalent Circuit for Photodiode

Figure A-2 shows the Thevenin equivalent circuit with the photodiode signal generator now represented as a voltage source E_o. According to Kirkoff's Law, the sum of all iZ drops around a closed loop is equal to the Emf. Therefore,

$$E_o = i\,(Z_d + Z_s + Z_\ell) \tag{A-1}$$

The current through the load is

$$i = \frac{E_o}{(Z_d + Z_s + Z_\ell)}. \tag{A-2}$$

Since $E_o = i_s Z_d$, where i_s is the short circuit signal current, we can write equation (A-2) as

$$i = i_s\left(\frac{Z_d}{Z_d + Z_s + Z_\ell}\right). \tag{A-3}$$

The IF signal power delivered to the load is

$$P_{IF} = \overline{i^2}\, R_\ell = \overline{i_s^2}\, R_\ell \frac{|Z_d|^2}{|Z_d + Z_s + Z_\ell|^2} \tag{A-4}$$

where straight brackets indicate the absolute value of a complex quantity. Defining the complex impedances as shown in Figure A-2, and substituting in equation (A-4) gives

$$P_{IF} = \overline{i_s^2}\, R_\ell \left| \frac{\left|\left(\frac{R_d}{1 + j\omega CR_d}\right)\right|}{\left(\frac{R_d}{1 + j\omega CR_d}\right) + (R_s + j\omega L) + R_\ell} \right|^2 \tag{A-5}$$

Now the problem is to rationalize the complex impedance terms and find the square of the absolute value. The complex impedance terms can be manipulated as follows.

$$\left| \frac{R_d}{(1 + j\omega CR_d)\left(\frac{R_d}{1 + j\omega CR_d} + R_s + j\omega L + R_\ell\right)} \right|^2 =$$

$$\left| \frac{R_d}{R_d + R_s + j\omega L + R_\ell + j\omega C R_d R_s - \omega^2 LCR_d + j\omega C R_d R_\ell} \right|^2 =$$

$$\left| \frac{1}{\left[1 + \left(\frac{R_s + R_\ell}{R_d}\right) - \omega^2 LC\right] + j\left[\frac{\omega L}{R_d} + \omega C(R_s + R_\ell)\right]} \right|^2 . \qquad \text{(A-6)}$$

This last equation is of the form $\left|\frac{1}{X + jY}\right|^2$. It can easily be shown that

$$\left|\frac{1}{X + jY}\right|^2 = \frac{1}{X^2 + Y^2}, \qquad \text{(A-7)}$$

so that equation (A-5) can now be written as

$$P_{IF} = \overline{i_s^2}\, R_\ell \left\{ \frac{1}{\left[1 + \left(\frac{R_s + R_\ell}{R_d}\right) - \omega^2 LC\right]^2 + \left[\frac{\omega L}{R_d} + \omega C(R_s + R_\ell)\right]^2} \right\}, \qquad \text{(A-8)}$$

or

$$P_{IF} = \overline{i_s^2}\, R_\ell F(\omega) \qquad \text{(A-9)}$$

Where $F(\omega)$ is a function which expresses the frequency dependence of the signal power due to circuit capacitance and inductance,

$$F(\omega) = \left\{ \left[1 + \left(\frac{R_s + R_\ell}{R_d}\right) - \omega^2 LC\right]^2 + \left[\frac{\omega L}{R_d} + \omega C(R_s + R_\ell)\right]^2 \right\}^{-1} . \qquad \text{(A-10)}$$

Appendix B

HETERODYNE NOISE EQUIVALENT POWER DERIVATION

The defining equation for the heterodyne noise-equivalent-power (NEP_H) of a photomixer is

$$NEP_H = \frac{P_s B}{(S/N)_p} \tag{B-1}$$

where P_s is the signal power incident on the photomixer, $(S/N)_p$ is the signal-to-noise power ratio, and B is the noise bandwidth. We are concerned here, not with the ideal case of the photomixer by itself, but with the practical situation of the photomixer connected to a load which is presumed to be the input impedance of a preamplifier. The signal-to-noise power ratio is that which is present at the preamplifier input terminals. This situation was discussed in Appendix A.

The electrical signal power produced by the photomixer at the IF and delivered to the preamplifier is, from equations (3), (9) and (A-9)

$$P_{IF} = \overline{i_s^2} R_\ell F(\omega)$$

$$P_{IF} = 2 I_{LO} I_S R_\ell F(\omega)$$

$$P_{IF} = 2\left(\frac{\eta e}{h\nu}\right)^2 P_{LO} P_S R_\ell F(\omega). \tag{B-2}$$

There are three sources of noise which must be considered; (1) dark current shot noise, (2) LO induced current shot noise, and, (3) preamplifier noise. The dark current shot noise power delivered to the preamplifier is

$$P_{n,s} = \overline{i_{n,s}^2} R_\ell F(\omega) B$$

$$P_{n,s} = 2 e I_d R_\ell F(\omega) B. \tag{B-3}$$

The LO induced shot noise delivered to the preamplifier is

$$P_{n,LO} = \overline{i^2_{n,LO}} R_\ell F(\omega) B$$

$$P_{n,LO} = 2eI_{LO} R_\ell F(\omega) B \tag{B-4}$$

The preamplifier noise is frequently expressed in terms of a noise figure or effective noise temperature. However, these parameters are well defined only for the case of matched source (photomixer) and load (preamplifier) conditions. This is definitely not the case for these photomixers whose impedance is mostly capacitive reactance and considerably greater than the preamplifier input impedance of 50 ohms. Additionally, the preamplifier noise will most likely be frequency dependent. Therefore, we will represent the preamplifier noise simply by the symbol $N_a(\omega)$ which is the measured value of noise power per unit frequency under actual operating conditions.

The total noise power can now be expressed as

$$P_{n,T} = [2eI_d R_\ell F(\omega) + 2eI_{LO} R_\ell F(\omega) + N_a(\omega)]B \tag{B-5}$$

The signal-to-noise ratio is equation (B-2) divided by (B-5)

$$\left(\frac{S}{N}\right)_p = \frac{2\left(\frac{\eta e}{h\nu}\right)^2 P_{LO} P_s R_\ell F(\omega)}{[2eI_d R_\ell F(\omega) + 2eI_{LO} R_\ell F(\omega) + N_a]B} \tag{B-6}$$

Inserting this in equation (B-1) we obtain the expression for heterodyne NEP

$$\frac{NEP_H}{B} = \frac{h\nu}{\eta}\left[1 + \frac{I_d}{I_{LO}} + \frac{N_a(\omega)}{2eI_{LO} R_\ell F(\omega)}\right]. \tag{B-7}$$

Standard Bibliographic Page

1. Report No.	2. Government Accession No.	3. Recipient's Catalog No.
NASA CR-4094		

4. Title and Subtitle	5. Report Date
Development of a P-I-N HgCdTe Photomixer for Laser Heterodyne Spectrometry	September 1987
	6. Performing Organization Code
7. Author(s)	8. Performing Organization Report No.
Peter R. Bratt	**62562**
9. Performing Organization Name and Address	10. Work Unit No.
Hughes Aircraft Company **Santa Barbara Research Center** **75 Coromar Drive** **Goleta, California 93117**	11. Contract or Grant No. **NAS1-16057**
12. Sponsoring Agency Name and Address	13. Type of Report and Period Covered
National Aeronautics and Space Administration Langley Research Center Hampton, VA 23665-5225	Contractor Report - Final
	14. Sponsoring Agency Code

15. Supplementary Notes

Langley Technical Monitor: W.E. Miller

16. Abstract

An improved HgCdTe photomixer technology was demonstrated employing a p-i-n photodiode structure. The i-region was near intrinsic n-type HgCdTe; the n-region was formed by B^+ ion implantation; and the p-region was formed either by a shallow Au diffusion or by a Pt Schottky barrier. Experimental devices in a back-side illuminated mesa diode configuration were fabricated, tested and delivered. The best photomixer was packaged in a 24-hour LN_2 dewar along with a cooled GaAs FET preamplifier. Testing was performed by mixing blackbody radiation with a CO_2 laser beam and measuring the IF signal, noise, and signal-to-noise ratio in the GHz frequency range. Signal bandwidth for this photomixer was 1.3 GHz. The heterodyne NEP was 4.4×10^{-20} W/Hz out to 1 GHz increasing to 8.6×10^{-20} W/Hz at 2 GHz. Other photomixers delivered on this program had heterodyne NEPs at 1 GHz ranging from 8×10^{-20} to 4.4×10^{-19} W/Hz and NEP bandwidths from 2 to 4 GHz.

17. Key Words (Suggested by Authors(s))	18. Distribution Statement
HgCdTe, Photomixer, Optical heterodyne detection	**Unclassified - Unlimited** Subject Category 76

19. Security Classif.(of this report)	20. Security Classif.(of this page)	21. No. of Pages	22. Price
Unclassified	Unclassified	60	A04

For sale by the National Technical Information Service, Springfield, Virginia 22161

NASA-Langley, 1987